

531 new spectroscopic redshifts from the CDFS and a test on the cosmological relevance of the GOODS-South field

C. D. Ravikumar^{1,2}, M. Puech¹, H. Flores¹, D. Proust¹, F. Hammer¹, M. Lehnert^{3,1}, A. Rawat^{4,1}, P. Amram⁵, C. Balkowski¹, D. Burgarella⁵, P. Cassata⁶, C. Cesarsky⁷, A. Cimatti⁸, F. Combes⁹, E. Daddi^{10,12}, H. Dannerbauer¹¹, S. di Serego Alighieri⁸, D. Elbaz¹², B. Guiderdoni^{13,2}, A. Kembhavi⁴, Y. C. Liang¹⁴, L. Pozzetti¹⁵, D. Vergani¹, J. Vernet⁷, H. Wozniak¹³, X.Z. Zheng¹¹

¹ GEPI, Observatoire de Paris-Meudon, 92195 Meudon, France, e-mail: Chazhiyat.Ravikumar@obspm.fr

² Institut d'Astrophysique du CNRS, 98 bis Boulevard Arago, F-75014 Paris, France

³ Max-Planck-Institut für extraterrestrische Physik, Giessenbachstrasse, 85748 Garching bei München, Germany

⁴ Inter University Center for Astronomy & Astrophysics, Post Bag 4, Ganeshkhind, Pune 411007, India

⁵ Laboratoire d'Astrophysique de Marseille, Observatoire Astronomique de Marseille-Provence, 2 Place Le Verrier, 13248 Marseille, France

⁶ Dipartimento di Astronomia, Vicoletto Osservatorio 2, I-35122, Padova, Italy

⁷ ESO, Karl-Schwarzschild Strasse 2, D85748 Garching bei München, Germany

⁸ INAF, Osservatorio Astrofisico di Arcetri, Largo Enrico Fermi 5, I-50125, Florence, Italy

⁹ LERMA, Observatoire de Paris, 61 Av. de l'Observatoire, 75014 Paris, France

¹⁰ National Optical Astronomy Observatory, 950 North Cherry Avenue, Tucson, AZ 85719

¹¹ MPIA, Königstuhl 17, D-69117 Heidelberg, Germany

¹² CEA Saclay/DSM/DAPNIA/Service d'Astrophysique, Orme des Merisiers, F-91191 Gif-sur-Yvette Cedex, France

¹³ Centre de Recherche Astronomique de Lyon, 9 Avenue Charles Andr, 69561 Saint-Genis-Laval Cedex, France

¹⁴ National Astronomical Observatories, Chinese Academy of Sciences, 20A Datun Road, Chaoyang District, Beijing 100012, China

¹⁵ INAF - Osservatorio Astronomico di Bologna, via Ranzani 1, 40127 Bologna, Italy

Received date; accepted \mid date \downarrow

ABSTRACT

Context. This paper prepares a series of papers analysing the Intermediate MAss Galaxy Evolution Sequence (IMAGES) up to a redshift of one. Intermediate mass galaxies ($M_J \leq -20.3$) are selected from the Chandra Deep Field South (CDFS) for which we identify a serious lack of spectroscopically determined redshifts.

Aims. Our primary aim in this study is therefore to obtain a sample of intermediate mass galaxies with known spectroscopic redshift to be used for further analysis of their 3D-kinematics. We also intend to test whether this important cosmological field may be significantly affected by cosmic variance.

Methods. The spectroscopic observations were carried out using VIMOS on the ESO VLT. The data reduction was done using a set of semi-automatic IRAF procedures developed by our team.

Results. We have spectroscopically identified 691 objects including 580 galaxies, 7 QSOs, and 104 stars. The overall completeness achieved is about 76% for objects with $I_{AB} \leq 23.5$ in the CDFS after excluding instrumental failures. This study provides 531 new redshifts in the CDFS. It confirms the presence of several large scale structures in the CDFS, which are found to be more prominent than in other redshift surveys. To test the impact of these structures in the GOODS-South field, we construct a representative redshift catalogue of 640 galaxies with $I_{AB} \leq 23.5$ and $z \leq 1$. We then compare the evolution of rest-frame U, B, V and K galaxy luminosity densities to that derived from the Canada France Redshift Survey (CFRS). The GOODS South field shows a significant excess of luminosity densities in the $z=0.5-0.75$ range, which increases with the wavelength, reaching up to 0.5 dex at $2.1 \mu\text{m}$. Stellar mass and specific star formation evolutions might be significantly affected by the presence of the peculiar large scale structures at $z=0.668$ and at $z=0.735$, that contain a significant excess of evolved, massive galaxies when compared to other fields.

Conclusions. This leads to a clear warning to results based on the CDFS/GOODS South fields, especially those related to the evolution of red luminosity densities, i.e. stellar mass density and specific star formation rate. Photometric redshift techniques, when applied to that field, are producing quantities which are apparently less affected by cosmic variance (0.25 dex at $2.1 \mu\text{m}$), however at the cost of the difficulty in disentangling between evolutionary and cosmic variance effects.

Key words. surveys: high-redshift - galaxies: distances and redshifts - galaxies: observations - cosmology: evolution - galaxies: large scale structure of Universe

1. Introduction

Studies suggest a growing evidence of significant evolution in the ensemble of galaxies out to $z = 1$. Analysis of stellar population of galaxies shows that the bulk of star formation occurs between $z = 1$ and $z = 0.4$, mostly dominated by star formation in galaxies in the range $3 - 30 \times 10^{10} M_{\odot}$ (Heavens et al. 2004; Hammer et al. 2005). This increased star formation activity is reflected in the strong evolution shown by galaxies in this redshift range from the analysis of the $15\mu\text{m}$ observations by ISOCAM (Elbaz et al. 2002). These infrared selected galaxies, with their high star formation rate, averaging $\sim 100 M_{\odot}/\text{yr}$, contribute significantly to the star formation history (Flores et al. 1999; Le Floc'h et al. 2005 and the references therein). The Luminous Infra-Red Galaxies (LIRGs) are up to 40 times more numerous at $z \sim 1$ than locally, and such a strong luminosity evolution has been attributed to rapidly increased frequency of interactions ($(1+z)^{3-4}$ for $z \leq 1$; see e.g. Hammer et al. 2005). However, major merging events appear to drive the high star-formation rates of only about 30% of LIRGs (Flores et al. 1999; Zheng et al. 2004). Interestingly, some of these star-forming galaxies appear to be large, massive disk galaxies, thus emphasizing the important role of studying the dynamics of intermediate mass ($3 - 30 \times 10^{10} M_{\odot}$) galaxies for understanding galaxy evolution.

Through the ESO large program “Intermediate Mass Galaxies Evolution Sequence (IMAGES)” we intend to (1) establish the evolution of mass-to-light ratio; (2) test the different physical processes leading to the present day Hubble sequence; (3) detail the star formation history of each individual galaxy; and (4) test the evolution of mass-metallicity relation, angular momentum, size, and mass. The analysis involves combining GIRAFFE and FORS2¹ observations, which are being carried out, of a sample of intermediate mass galaxies, selected mainly by their rest-frame J_{AB} magnitude, and importantly, with the largest multi-wavelength photometric data available. The 3D spectroscopic observations using GIRAFFE (e.g. Flores et al. 2004) can provide detailed kinematics (e.g. Puech et al. 2006a) including accurate Tully-Fisher relations (Tully & Fisher 1977, see Flores et al. 2006). It can also provide electron density maps of distant galaxies (Puech et al. 2006b), thanks to the high spectral resolution ($R \sim 10000$) of the instrument allowing the $[\text{OII}]\lambda\lambda 3726, 3729$ doublet to be easily resolved. Besides this, we will derive the chemical abundances of galaxies using observations with FORS2 (Appenzeller et al. 1998), taking advantage of its excellent red sensitivity.

The sample of intermediate mass galaxies for our study IMAGES is selected mainly by their rest frame J_{AB} magnitudes ($M_J(AB) \leq -20.3$) corresponding to stellar masses greater than $1.5 \times 10^{10} M_{\odot}$. Because the CDFS represents one of the most deeply surveyed at all wavelengths, we have chosen to carry out IMAGES in this field. Unfortunately, in the CDFS, this galaxy population had insufficient numbers of spectroscopic redshifts available. The VVDS (Vimos VLT Deep Survey, Le Fèvre et al. 2004), FORS2 (Vanzella et al. 2005, 2006) and K20 (Mignoli et

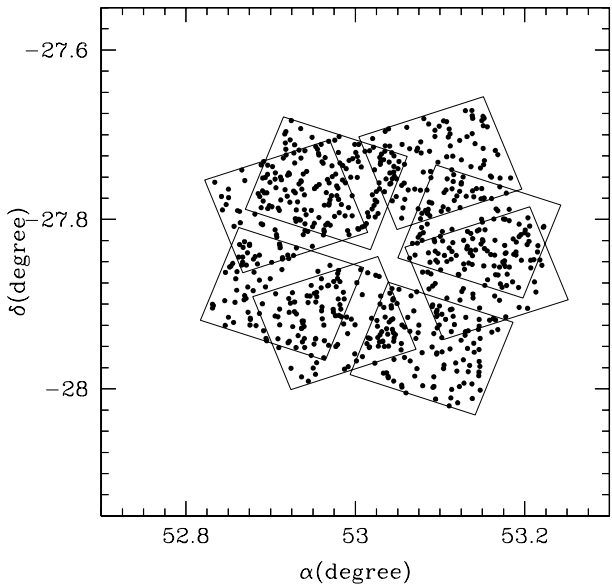


Fig. 1. The two pointings by VIMOS in the CDFS for observation with a similar strategy than VVDS. The black dots are the positions of the objects for which we have determined redshifts. A sample of 969 objects with $I_{AB} \leq 23.5$ were selected for observation constituting $\sim 25\%$ of galaxies on the field.

al. 2005) surveys were intentionally designed to focus on faint magnitudes (typically $I_{AB} \leq 24$) in order to preferentially identify objects at higher redshifts which results in essentially picking up fainter (and hence low mass) objects in the redshift range ($0.4 \leq z \leq 0.9$) we are interested in. With the redshift survey discussed here, we intend to increase the number of redshifts of relatively bright and emission line galaxies. To study the evolution of galaxies in a particular field, one must pay careful attention to how representative the field is, for example, in its redshift distribution. The existence of one or several significant peaks in the redshift distribution of the CDFS, indicating the presence of large scale structures, might be problematic in interpreting the results when studying galaxy evolution, such as in GOODS or IMAGES programs.

The structure of the paper is as follows: In §2 we describe the observation and data reduction of low-resolution VIMOS spectra from the CDFS and in §3 we provide the general properties of the sample for which we obtain redshifts. Further, we analyze the cosmological relevance of GOODS in §4 by constructing a representative spectroscopic catalog paying attention to the selection biases involved. Finally, we provide a conclusion in §5. We adopt the Λ -CDM cosmological model ($H_0 = 70 \text{ km s}^{-1}\text{Mpc}^{-1}$, $\Omega_M = 0.3$ and $\Omega_{\Lambda} = 0.7$). Also, all magnitudes used in this paper are in AB system, unless explicitly noted otherwise.

Send offprint requests to: Ravikumar

¹ For a description of the instruments, GIRAFFE & FORS2, see <http://www.eso.org/instruments/>

2. Observations

We have carried out the spectroscopic observations with VIMOS on the VLT-UT3 Melipal during December 3-4, 2004. The observing conditions were photometric and the seeing was ~ 1 arcsec. The low resolution red grism, LRRED, was used with a slit width of 1 arcsec. The spectral resolution in this mode is 34\AA at 7500\AA or $R \sim 220$. The red bandpass filter, which also serves for order separation, limits the spectral range to $5500 - 9500\text{\AA}$. A complete VIMOS pointing consists of observations with four quadrants of the instrument each separated by about 2 arcmin from its neighbor. We have set two pointings around the CDFS as shown in the Fig. ?? with an angle of ~ 90 degrees between them. The total area covered is ~ 370 arcmin 2 on the sky. An integration time of 45 minutes was given per pointing. Given the short exposure time, we have concentrated the slits mainly on galaxies of the field with $I_{AB} \leq 23.5$ in order to complement the existing deeper surveys. The positions of the objects for which we could estimate redshifts are also shown in Fig. ??.

The preparation of the slit masks was done using the photometric catalog from ESO Imaging Survey (Arnouts et al. 2001) and the I-band VIMOS pre-images. The VMMPS code² was run to optimize the number and positions of the slits for each quadrant. However, we have carried out a final re-arrangement of the slits by hand in order to improve the number of objects observed. This resulted in placing a total of 1142 slits in the two pointings, among them 969 were associated with objects with $I_{AB} \leq 23.5$.

Data reduction and extraction of the optical spectra were performed by three of us (CDR, HF and DP) using a set of semi-automatic IRAF³ procedures developed by our team. The routines allowed us to reconstruct simultaneously the spectra of the object and the surrounding sky. The spectra were flux-calibrated using two standard stars. Images in the V, R and I bands were used to check the slope of our spectra.

2.1. Redshifts

The redshift determination of each spectrum from all the eight quadrants was done independently by three team members (CDR, HF & DP), making sure that each spectrum is analysed by at least two members. When the individual estimates of the redshifts among the three members did not agree, measurements were examined by a fourth team member (FH). When the fourth team member agrees with neither of the previous independent estimates, that object is discarded. Each redshift measurement is associated with a ‘quality’ flag denoting the reliability of the extraction. Given the low signal-to-noise, mainly due to the short total integration time, we have classified the reliability into four classes; secure (class=2), insecure (1), single emission line (9) and failed (0) observations. Secured spectro-

² <http://134.171.56.104/observing/p2pp/OSS/VMMPS/VMMPS-tool.html>

³ IRAF is distributed by the National Optical Astronomy Observatories, which are operated by the Association of Universities for Research in Astronomy, Inc., under cooperative agreement with the National Science Foundation.

Table 1. Number and type of objects in the classes, secure (2), insecure (1) and single emission line (9), for which we have determined redshifts. The % is the percentage of objects for which redshifts are obtained out of 1142 slits placed. For about 12% of objects we were not able to determine the redshift because of instrument-related problems. See text for more details.

Class	Galaxy	Star	QSO	Total	%
2	308	88	6	402	35.2
1	206	16	1	223	19.5
9	66	–	–	66	5.8
Total				691	60.5

scopic identifications contain more than two strong features, while sources classified as insecure contain either a strong feature with not very reliable supporting features, or multiple features not strong enough to confirm the redshift, giving a confidence of about only 50% to the estimated redshift. Class (9) sources correspond to spectra with a single strong emission line without any other features. Redshifts are assigned tentatively for such cases. Typically this is the case where we are unable to identify between [OII] $\lambda 3727$ and H α emission lines. The failed class contains spectra for which we could not obtain a redshift, mainly due to low signal-to-noise or to reasons that have an instrumental origin, like the presence of bad pixels or object being near the boundary of the slit. Figure 2 shows the sample spectra for the different classes used. In addition to this we have provided each redshift with a type classification to show the observed spectrum belongs to an emission line galaxy (type=1), an absorption line galaxy (2), a quasar (3), or a star (4).

2.2. The redshift catalog

The catalog lists spectroscopic data on 691 objects from the CDFS, containing 580 galaxies, 104 stars and 7 QSOs (see Tables 1 and 2). The catalog can be downloaded from the CDS website. In the catalog we provide for each object:

- The ESO imaging survey (EIS) identification number and equatorial coordinates (equinox 2000);
- The class and type codes denoting the quality and nature of the spectra, as described in the previous section;
- The redshift measured by the IMAGES team;
- The internal identifier;
- The isophotal I_{AB} band magnitude from Arnouts et al. (2001), and the derived absolute magnitudes (AB system) following Hammer et al. (2005) on the basis of available EIS photometry; M_U values have been calculated on the basis of observed V and V-I to allow comparison with CFRS values (see section 4.3), and then might be affected by systematics at low redshift.

3. Description of the IMAGES catalog

Out of the 1142 slits placed, we could estimate redshifts for 691 objects, giving a success rate of $\sim 61\%$. Taking into account

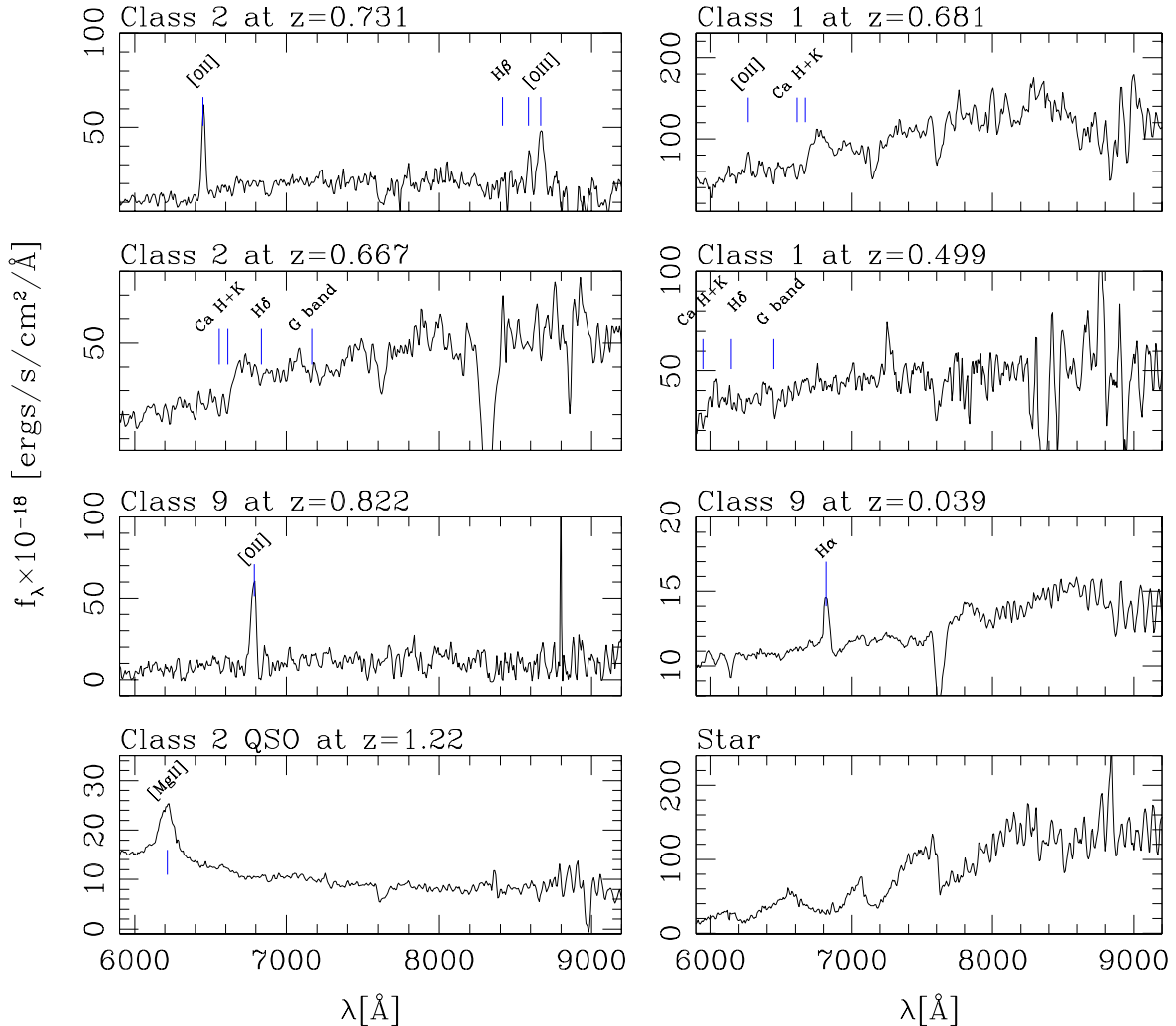


Fig. 2. Classification of spectra based on their quality. Sample spectra of various type and quality (Class 2: secure, class 1: insecure, class 9: single line). (**From top to bottom:**) emission line galaxies, absorption line galaxies, single emission line galaxies. (**Bottom:** AGN and star).

the 969 objects with $I_{AB} \leq 23.5$, we successfully estimate the redshift of 635 of them (success rate of 66%). The failure to estimate a redshift is associated mainly to low signal to noise ($\sim 26\%$), objects falling near the edge of the slit ($\sim 11\%$), and presence of column of bad pixels ($\sim 2\%$).

We have observed 12 galaxies twice. By taking the difference of the two individual independent redshift measurements, we find a systematic uncertainty of 0.006 ± 0.014 in our redshift estimates. With the limited statistics available, we estimate a very conservative upper-limit to the dispersion in our redshifts of 0.010.

In Fig. ?? we show the distribution of the redshifts for all galaxies and QSOs in our sample, consisting of all classes 2, 1, and 9. The mean and median of the distribution are 0.643 and

0.665 respectively. The strongest peaks in redshift are at 0.670 (82 objects, with $\Delta z = \pm 0.020$), at 0.735 (58) and at 0.210 (23). The first two peaks are in agreement with the existence of ‘wall-like’ structure in the CDFS (Le Fèvre et al. 2004; Gilli et al. 2003, Vanzella et al. 2005).

3.1. Completeness

The spectroscopic completeness, i.e. the ratio of the actual number of spectroscopic identifications obtained to that of total number of objects observed spectroscopically as a function of magnitude, helps in understanding the magnitude dependent bias of the sample. As mentioned previously, for objects with $I_{AB} \leq 23.5$, the overall spectroscopic completeness is 66%. If

Table 3. Comparison of the number (N) of galaxies (and AGN) with redshifts available in CDFS as a function of I_{AB} limiting magnitudes. Our study represents from 20 to 35% of galaxy redshifts available in the CDFS. The last column shows the number of galaxies observed in common from one survey to the others, based on the cross correlation of targets in the CDFS. 136 galaxies and 24 stars in IMAGES are found in common with other surveys, leaving us with $587 - 136 = 451$ unique identifications of galaxy redshifts and $691 - 160 = 531$ unique objects in IMAGES.

Sample	Time ^a	$I_{AB} \leq 22.5$	$I_{AB} \leq 23.5$	$I_{AB} \leq 24$	All	Common
K20	-	169	236	256	459	133
VVDS	265	552	1089	1460	1460	223
FORS2	281	127	219	308	711	144
Szokoly	114	77	89	90	121	55
IMAGES	45	376	532	569	587	136
Unique Identifications						
ALL	-	1068	1846	2328	2781	-
IMAGES	-	280	401	435	451	-
% ^b	-	35.5	27.8	23.0	19.4	-

^a Approximate average exposure time per slit in minutes. The higher integration times used by other studies were justified by their scientific goals.

^b The percentage of galaxies with new redshift identifications from the IMAGES survey. Calculated as IMAGES/(ALL - IMAGES).

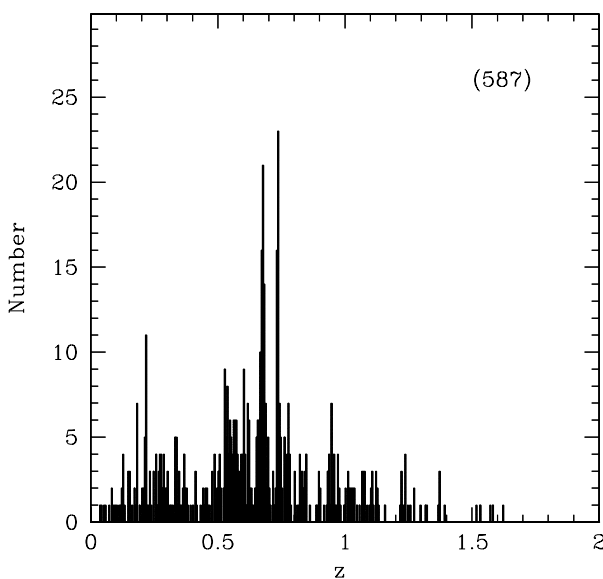


Fig. 3. Histogram of redshifts for galaxies and QSOs in our sample, comprising of all classes 2,1, and 9. The size of the redshift bin is 0.005. The distribution shows prominent peaks at 0.210, 0.530, 0.670, and 0.735.

we exclude the failures that have an instrumental origin, then the spectroscopic completeness for $I_{AB} \leq 23.5$ objects is 76%. In Fig. ??, we show the spectroscopic completeness achieved in measuring redshifts as a function of the apparent magnitude (I_{AB}). In the upper panel the histogram of observed targets with $I_{AB} \leq 23.5$ are shown in white, while the black, green and blue histograms show the magnitude distribution of objects with redshift class 2, 1 and 9, respectively. Further, in Table 3, we show a comparison of the number of galaxy redshifts deter-

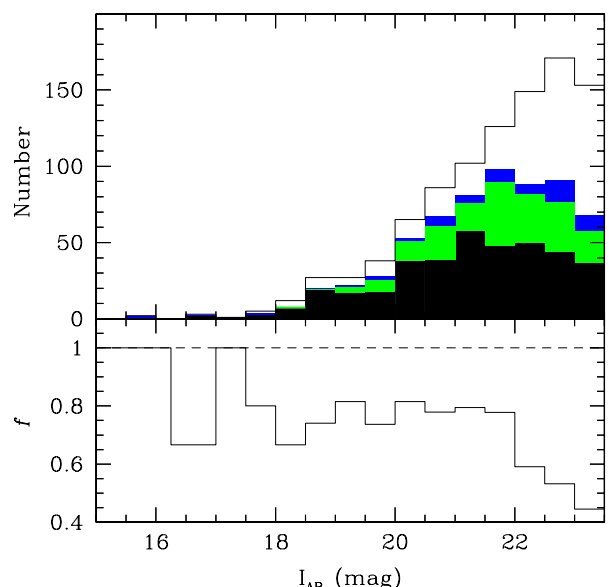


Fig. 4. Redshift measurement completeness for $I_{AB} \leq 23.5$ sample in IMAGES. In the upper panel, we show the magnitude distribution of objects with a redshift class 2 (black), 1 (green), and 9 (blue), along with that for the observed targets (open). The lower panel shows the histogram of the fraction (f) of objects with redshifts compared to the total observed from IMAGES. We measure redshifts for 66% of the target objects, while the completeness achieved is 76% when we exclude failures that have an explicit instrumental origin.

mined by IMAGES with the K20, VVDS, FORS2, and Szokoly et al. (2004). We have taken into account only reliable redshifts, with a confidence of at least 50%. This means that redshift estimations with flags 1, 2 & 9 from IMAGES, flags 1-4 & 9 from

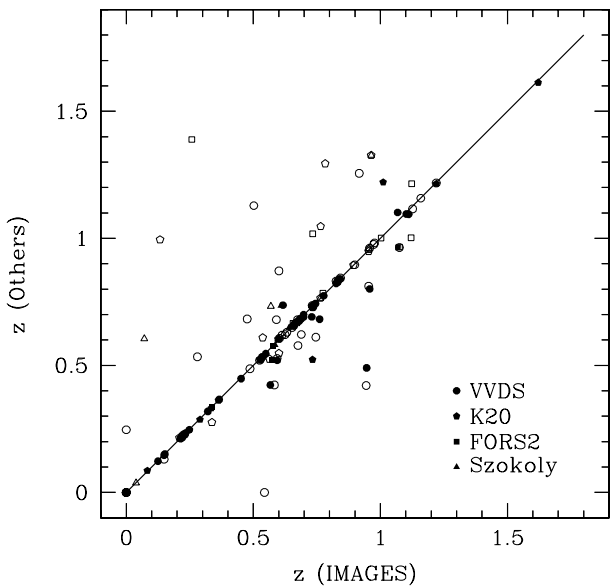


Fig. 5. The comparison of our redshift estimation with VVDS (open and shaded circles), K20 (open and shaded pentagons), FORS2 (open and shaded squares), and Szokoly (open and shaded triangles). The open symbols identify objects for which at least one of the survey considers the redshift as insecure (for example, with flags 1 and 9 in both IMAGES and VVDS), otherwise a full symbol is adopted.

VVDS, flags 0 & 1 from K20, all from FORS2⁴. The high efficiency coupled with the relatively high completeness attained over a short exposure time highlights the advantage of low resolution spectroscopy by VIMOS in estimating redshifts up to $z = 1.5$.

3.2. Comparison with other redshift estimations in the CDFS

We have compared our redshift estimations with those publicly available in the CDFS, i.e., the VVDS (Le Fèvre et al. 2004), K20 (Cimatti et al. 2002), FORS2 (Vanzella et al. 2005, 2006) and the X-ray selected sample of Szokoly et al. (2004). We have observed 98, 42, 22, and 18 objects in common to the VVDS, K20, FORS2 and Szokoly et al. samples, respectively. Because former surveys also include target duplications, we find that 160 IMAGES objects were already observed in for-

⁴ Note that the flags used by Vanzella et al. are not exactly similar to that used by other surveys., and flags 0.5, 1, 2 & 3 from Szokoly et al. were selected in Table 3. We note that our study (IMAGES) represents approximately 28% of the reliable redshifts for galaxies with $I_{AB} \leq 23.5$ in the CDFS. Excluding redshifts of objects already identified by other surveys (repeated observations, see Table 3), the IMAGES catalogue produces 531 new redshift identifications, consisting of 307, 170 and 54 objects with class codes 2, 1, and 9. The numbers of galaxies, stars and quasars present in this catalog are 447, 80 and 4, respectively.

mer surveys. For 76% of the common elements with VVDS, we have $\frac{\Delta z}{(1+z)} \leq 0.01$. The distribution of redshift difference for 56 objects where both VVDS and IMAGES mark a secured estimation, shows $\sigma_{\Delta z} = 0.069$. We obtain similar percentages and dispersions for other samples also. In Fig. ?? we show the comparison of our redshift estimation with VVDS (circle), K20 (pentagon), FORS2 (square) and Szokoly et al. (triangle) samples. The shaded and open symbols are used to represent secure and insecure estimations. Clearly, all the significant differences are arising from low quality of the spectra in at least one of the surveys. Two of us (CDR & HF) compared the spectra of objects for which we obtained significantly different redshifts from VVDS, using the CENCOS database⁵. After comparison, we have kept our redshift for about 60% of them. When spectral features did not match with the VVDS ones (all with very poor quality), we preferred our estimates because it appeared likely that the features in the VVDS spectra are artificial and arise from a failure by their automated data reduction in handling accurate sky subtraction and/or wavelength calibration. This was always possible anyway, since the VVDS team themselves assigned the sources that we find to have discrepant redshifts as of very poor quality. The redshift estimation for the object EISJ033235.64-274633.0 is noteworthy. We estimate a redshift of 0.564 while the VVDS team reports 3.6664 (GOODS identification J033235.62-274632.8) with their quality flag 2. We find the [OII] $\lambda 3727$ emission at 5837.9 Å, though with a class=1 as no more strong features are observed. The B band detection of the object ($B = 24.11$) also suggests an absence of the Lyman break feature corresponding to $z = 3.6664$, thus supporting our estimation of the lower redshift. This just highlights that caution should be observed when using redshift estimates of marginal or poor quality.

3.3. Stars and galaxies in the color-color diagram

The color-color diagram, provides an easy tool in identifying possible mis-classifications of stars and galaxies. However, there may be an overlap between the colours of stars and galaxies, especially for the bluest objects (e.g., Crampton et al. 1995). In Fig. ??, the variation of B-I as a function of I-K is shown. Filled triangles and squares show stars and galaxies with secure spectroscopic identifications, while the open symbols represent the same classes for objects with less secure identifications. Using the diagram, we selected objects for visual examination, wherever possible, through the available HST-ACS and the GEMS images. We noticed 26 (4% of total objects with spectroscopic redshift) obvious cases of galaxies identified as stars (insecure, with class 1) in the preliminary catalog. Due to this uncertainty induced by inspecting the images, the quality flag of these objects were degraded to unidentified (class 0) in the final catalog.

3.4. Magnitude distribution

The variation of the apparent I magnitude as a function of redshift for the galaxies in our IMAGES catalog is shown in Fig.

⁵ <http://cencosw.oamp.fr/FR/index.fr.html>

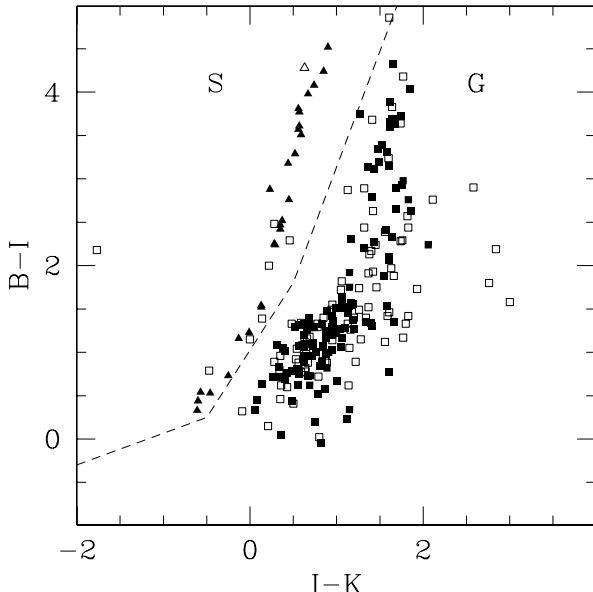


Fig. 6. The I-K vs. B-I diagram for stars (triangles) and galaxies (squares) with spectroscopic redshift measurements from IMAGES. Filled and open symbols represent secure and insecure redshift estimates respectively. The dashed line delineates roughly the regions occupied by stars (S) and galaxies (G).

???. Filled squares represent secure redshift identification while the insecure redshift estimates are shown by open squares. We have estimated the absolute magnitude following the method outlined in Hammer et al. (2001 & 2005). The distribution of absolute magnitude (M_B) versus redshift is shown in Fig. ???, indicating the absolute magnitude depth attained by our observations. For clarity, the brighter ($I_{AB} \leq 23.5$) and fainter ($I_{AB} > 23.5$) objects are represented by filled and open circles respectively.

3.5. The sample of emission line galaxies in the IMAGES survey

One of the main criteria for selecting our sample of intermediate mass galaxies, is the absolute magnitude selection $M_J \leq -20.3$. Such a limit corresponds to a stellar mass of $1.5 \times 10^{10} M_\odot$ when converting the J band luminosity using the prescription discussed in Bell et al (2003; see also Hammer et al, 2005). However, the near infrared observations in J , H , and K , essential for estimating M_J using the method of Hammer et al. (2005), are currently available only for the GOODS area, which forms a subset of the larger CDFS. But we find for galaxies in our sample with both B and J magnitudes, about 95% of $M_B \leq -20.0$ galaxies have $M_J \leq -20.3$. We obtained very similar percentage with a much larger sample of galaxies with photometric redshift (from COMBO-17, see Wolf et al, 2004). The latter test was conducted in order to verify that the selection biases involved in our sample (also see § 4.1) do not affect the fraction of $M_J \leq -20.3$ galaxies that could have $M_B > -20$.

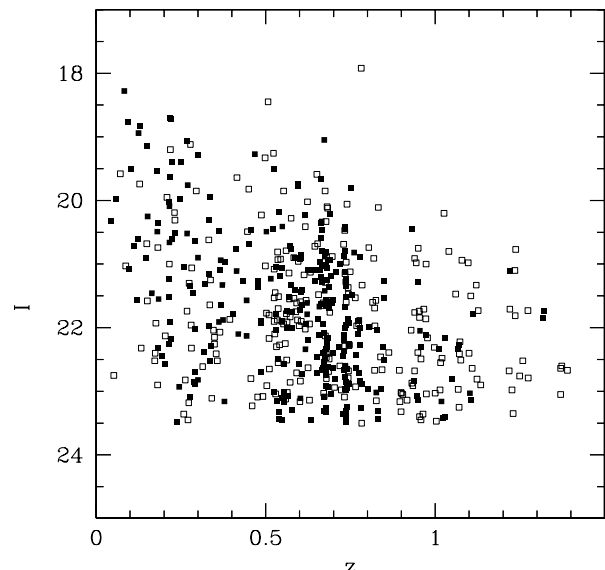


Fig. 7. The variation of the apparent I magnitude as a function of redshift, for galaxies for which redshifts are measured by the IMAGES survey. Filled and open squares show secure and insecure redshift estimates respectively.

Hence for emission line galaxies falling outside the area covered by the GOODS, we select our sample using $M_B \leq -20.0$ criterion. In Fig. ??, we show the histograms of emission line galaxies available in CDFS. The IMAGES survey identifies 69 galaxies with $M_J \leq -20.3$ and [OII] $\lambda 3727$ emission lines observable through GIRAFFE (blue dotted line), while 68 are available from the VVDS survey (black dashed line). We also identify 157 emission line galaxies with $M_B \leq -20.0$ for further observation, thus providing large enough sample of target galaxies for detailed analysis, as envisaged in the IMAGES program.

In what follows we provide a representative sample of galaxies with spectroscopic redshift in the GOODS field to address the issues related to the possible cosmological variance within this field.

4. The Representativeness of GOODS-South for Cosmological Studies

The GOODS project envisages the use of the best and probably the deepest multi-wavelength data in order to understand various cosmological problems, like the formation and evolution of galaxies and active galactic nuclei, and the distribution of dark matter and the large scale structure at high redshifts. However, after this region was chosen, it has been discovered that it had a “wall-like structure” (Le Fèvre et al. 2004; Gilli et al. 2003, Vanzella et al. 2005). Finding such a correlation in the galaxy distribution necessitates a more detailed analysis of issues related to the cosmological variance that might impact our understanding of galaxy evolution when using data from

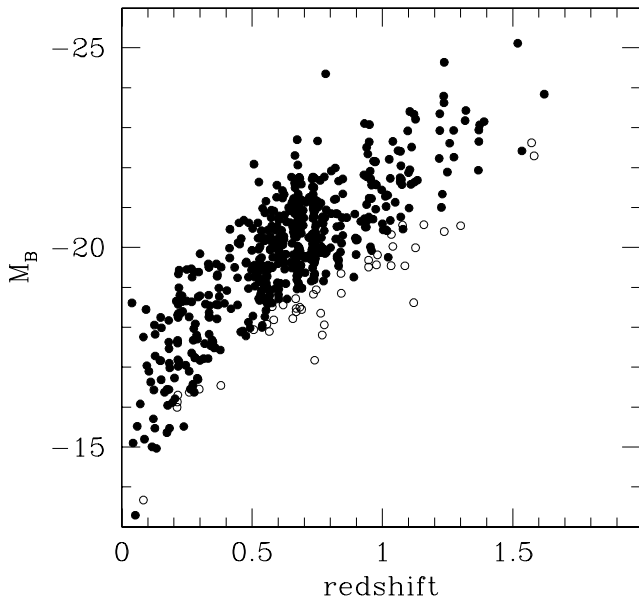


Fig. 8. Redshift vs absolute M_B magnitude for objects in our sample showing the depth attained by our observation. Objects brighter and fainter than $I_{AB} = 23.5$ are shown as filled and open circles respectively.

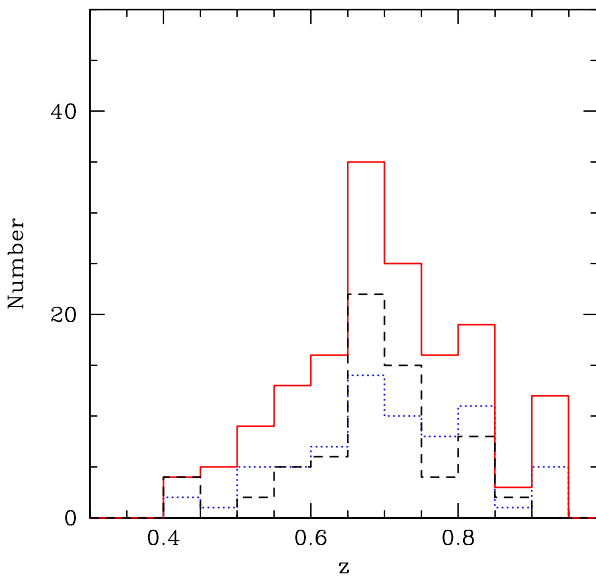


Fig. 9. Sample of galaxies that are candidates for GIRAFFE follow-up observations. The blue dotted histogram shows $[\text{OII}]\lambda 3727$ emission galaxies with $M_J \leq -20.3$, identified from the IMAGES survey while the black dashed histogram shows that from VVDS. The histogram with continuous red line shows the distribution of emission line galaxies with $M_B \leq -20.0$ but with no M_J data available. See text for more details.

the CDFS region. To conduct this investigation, we constructed a sample of galaxies with reliable spectroscopic redshifts in the GOODS area by combining the IMAGES data with other relevant publicly available spectroscopic redshift surveys. The sample is then used to compare the global properties of galaxies observed in the CFRS. The CFRS (see Crampton et al. 1995) is a collection of data and analysis on galaxies with $I_{AB} < 22.5$, selected in an unbiased way from 5 distinctly uncorrelated areas of 100 arcmin^2 in the sky to mitigate against the effects of cosmic variance (see Crampton et al. Figure 8 showing the redshift distribution of the 5 individual fields). This, though significantly less deep than the observations in the GOODS, the CFRS provides an ideal sample to test the possible impact of cosmic variance in the GOODS region.

4.1. The GOODS - South field spectroscopic catalogue: 640 galaxies with $I_{AB} \leq 23.5$ and $z \leq 1$

Though the IMAGES survey was highly efficient in estimating redshifts, the short integration time of the survey introduces a real bias towards brighter galaxies. This is evident in Fig. ?? as the fraction of redshift identified objects becomes low at fainter magnitudes ($I > 22$). Moreover, the high efficiency of the IMAGES survey is mainly reflected in its ability to obtain redshifts for galaxies with strong emission line spectra. The short integration time results in low signal-to-noise for faint objects which in turn causes serious difficulties in estimating redshifts of galaxies showing absorption line only or weak emission lines. Thus we tend to be particularly biased against obtaining redshifts the fainter early-type galaxies. On the other hand, we find that the selection criteria employed by the FORS2 team lead to spectroscopically identify those objects that are largely missed by IMAGES. The FORS2 spectroscopic team generally selected redder and fainter galaxies significantly helping to overcome the biases in our spectroscopic survey. The VVDS catalog forms a more complete sample (84% completeness for objects with $I_{AB} \leq 24$).

Here we limit our analysis to GOODS-South galaxies with $I_{AB} \leq 23.5$ and $z \leq 1$, with the aim of testing the cosmological relevance of the GOODS-South field within that redshift range. Fig. ?? compares properties of galaxies in VVDS (337 galaxies) to those of the combined sample of IMAGES and FORS2 (303 galaxies). It reveals a remarkable consistency between the two samples, which photometric, color and redshift distributions are almost indistinguishable one from the other on the basis of statistical tests. In the following we combine the two catalogues, assumed to provide a representative sample of $z \leq 1$ galaxies up to $I_{AB} = 23.5$. In the following, the GOODS - South field spectroscopic catalogue corresponds to the combination of the VVDS and of IMAGES and FORS2 catalogues in the GOODS field.

4.2. Comparison of the GOODS-S redshift distribution to that of GOODS-N, VVDS02h and CFRS

We have retrieved from the literature existing redshift surveys of similar depths than our GOODS-S sample. Fig. ?? presents

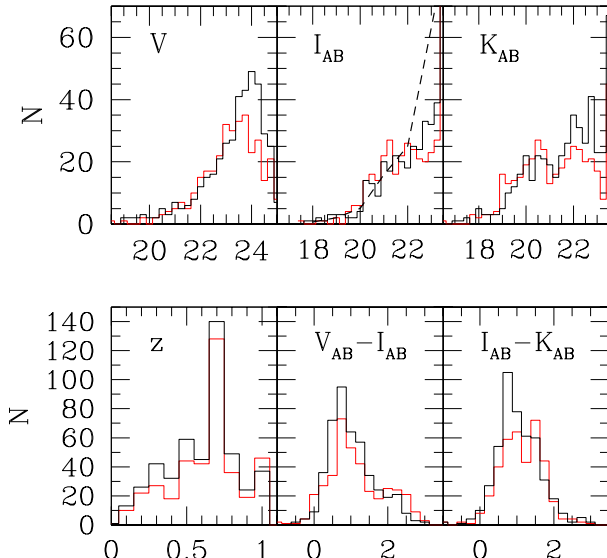


Fig. 10. Comparison between the distribution of VVDS (black histogram) and IMAGES+FOR2 (red histogram) galaxies in the GOODS field. From left to right, top to bottom, the two distributions are compared in V , I_{AB} , K_{AB} , z , $(V - I)_{AB}$ and $(I - K)_{AB}$, respectively. Kolmogorov-Smirnov tests show that the associated probabilities (for the two samples to be derived from the same population) are 96, 99.999, 82, 78, 96 and 99.999%, respectively. Notice that a Pearson test provides similar numbers (probabilities always larger than 91%). The dashed line in the top-middle panel represents the counts in the I band (see Arnouts et al, 2001), showing that both catalogues are missing galaxies at the faint end.

the 4 redshift histograms, revealing in three cases (GOODS-S, GOODS-N and VVDS02h) the existence of large scale structures. As noticed above, the CFRS is a blend of 5 different fields of view, so the combination has smeared the large scale structures. For each field we identified the two most prominent structures (in yellow), and identify the redshift area (in blue) surrounding the structure, which contains the same number of galaxies than the two structures. This is similar to an “equivalent (redshift) width” revealing the impact of the structure in a given redshift survey. The two prominent structures in GOODS-S, GOODS-N and VVDS02hr provide equivalent (redshift) widths of $\Delta z = 0.317, 0.148$ and 0.09 , respectively. It is unlikely that these differences can be related to the (small) differences in limiting magnitudes. Knowing that many studies of the evolution of integrated quantities such as SFR or stellar mass densities are considering redshift bins of Δz from 0.25 to 0.5 , this clearly requires more investigations to understand if GOODS-S field can be biased by the presence of such prominent large scale structures. In the following, we will test their impact in deriving luminosity density, by comparing with the CFRS, which is by construction, not affected by structures.

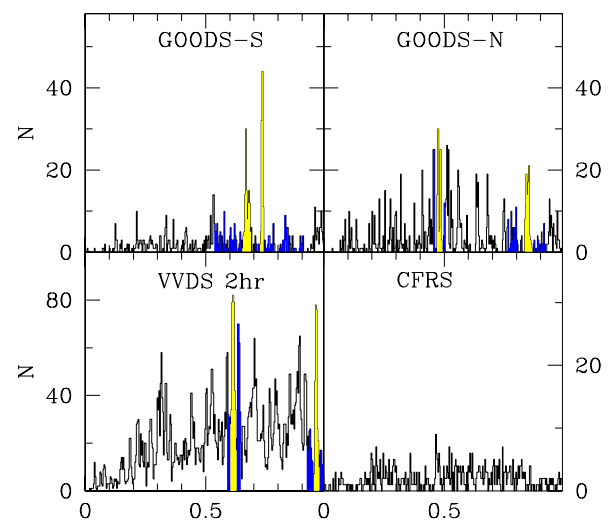


Fig. 11. Comparison between the redshift distribution of GOODS-S ($I_{AB} \leq 23.5$, this paper) redshift distribution to that of GOODS-N ($R_{AB} \leq 24.5$, Wirth et al, 2004), VVDS02h ($I_{AB} \leq 24$, Le Fevre et al, 2005) and CFRS ($I_{AB} \leq 22.5$, Crampton et al, 2005). In yellow are shown the two most prominent structures in GOODS-S, GOODS-N and VVDS02h. In blue are identified the redshift area surrounding the structure, which contains the same number of galaxies than the two largest structures.

4.3. Comparison of the luminosity evolution from GOODS-S with that from CFRS

The CFRS sample was selected solely by the $I_{AB} \leq 22.5$ criterion and includes 591 galaxies, among which 576 have $z \leq 1$. The GOODS spectroscopic catalog contains 428 $I_{AB} \leq 22.5$ galaxies, including 405 with $z \leq 1$. The number of objects with $I \leq 22.5$ forms about 49% of those present within this magnitude limit in the GOODS area and Fig. ?? (see upper middle panel) shows that it is a fair representation of $I \leq 22.5$ galaxies. In Fig. ?? we show the redshift variation of the ratios of luminosity densities of observed galaxies from the GOODS catalog with that from the CFRS, for galaxies with $0.25 \leq z \leq 1$, using 3 redshift bins. Recall that luminosity densities are evaluated from integrating the luminosity functions, which are themselves estimated from the distribution of observed galaxies. Any difference between the distribution of observed galaxies in two distinct areas, would undoubtedly generate similar difference in the derived luminosity densities. Fig. ?? proves that GOODS-South field displays a strong excess of luminosity densities in the $z=0.5-0.75$ bin, at B , V and especially at K wavelengths. We interpret this as related to large scale structure (i.e. cosmic variance) because more than half of the GOODS-South galaxies in that bin are found in two large scale structures (see Fig. ??). Besides this, the shape of the U luminosity

density evolution is far less affected, providing that star formation rate density from UV light is almost comparable from GOODS-South to CFRS. Nevertheless, Fig. ?? suggests that one has to be cautious in interpreting evolution of the stellar mass density on the sole basis of the GOODS-South or the CDFS galaxies, since it is particularly related to the K luminosity density evolution. In the next section, we test more accurately why the large scale structures in GOODS-South preferentially affect red luminosity densities rather than those at blue wavelengths.

To understand whether the cosmic variance related to the CDFS/GOODS-South field might affect analyses of galaxy evolution, Fig. ?? also displays (dashed lines) the same comparison with CFRS, but with adopting photometric redshifts rather than spectroscopic ones. Photometric redshifts are retrieved from Wolf et al. (2004) and are within the most used and accurate values existing for this field. Interestingly, most of the signature of the large scale structures disappear in the intermediate bin, except a signal in the K band. An examination of the distribution of photometric redshifts (see Wolf et al.' Figure 10) shows indeed that the large scale structures are somewhat recovered, but are much less prominent than in Fig. ?? (upper-left panel). For example, with photometric redshifts, the two prominent structures at $z=0.670$ and $z=0.735$ have merged, and the corresponding "equivalent width" is $\Delta z \sim 0.08$, to be compared to $\Delta z = 0.317$ when using spectroscopic redshifts. Thus, we wonder if some of the evolutionary trends found using photometric redshift surveys cannot be misunderstood as related to CDFS large scale structures.

4.4. Evolution of galaxies inside and outside the structures in the GOODS.

It is well understood that the environments in which galaxies reside have significant influence on their formation and evolution. To analyze the properties of galaxies inside and outside the structures, we designate galaxies in the field and in the structures as shown in Fig. ??a. The redshift range for field galaxies were selected so that each sample contains similar numbers of galaxies while the structures were defined solely as regions with significant excesses. In the other subpanels of Fig. ??, we show the distribution of U, V, and K luminosities of galaxies inside and outside the redshift spikes. The two distributions in U are not significantly different, overall suggesting a similarity in their star-formation rates. However, for K, there is significant difference in the distributions as the galaxies in the structures are likely to be more massive on average, while in the case of the comparison of the V-band luminosities, there is a difference, but it is statistically weaker. Testing each distribution with a Kolmogorov-Smirnov statistic confirms our visual impression, suggesting that the significance of the similarity in each pairs of histograms is 73, 2, and 0.6% for U, V, and K respectively. This implies that the distribution of K-band magnitudes is significantly different, the V-band magnitude distributions are only marginally different, and the U-band magnitude distribution are statistically the same. It is particularly interesting to note that the (UV traced) star formation rate does not dif-

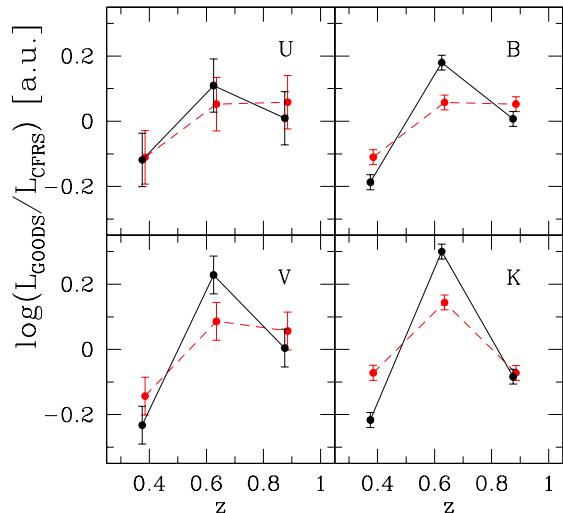


Fig. 12. Evolution of ratios of luminosity densities of observed galaxies from the GOODS spectroscopic sample and observed galaxies from CFRS as a function of redshift, for 3 redshift bins (0.25-0.5; 0.5-0.75 and 0.75-1). Calculations of absolute luminosities have been done following Hammer et al (2005). There is no noticeable variation in the evolution of U luminosity density between the samples, while the B, V and K light shows increasingly significant variations. We find the presence of large scale structure in the GOODS responsible for this. For consistency reason we derived the K_{AB} band luminosities in CFRS using $K_{AB} = K' + 1.87$ (as in GOODS), instead of $K_{AB} = K' + 1.78$ used in Lilly et al. (1995). Dashed (red) lines show a similar relation, but with adopting photometric redshifts from Wolf et al (2004) instead of spectroscopic redshifts. Error bars correspond to Poisson statistics combined with photometric errors from measurements (see Arnouts et al, 2001) and from calculations of the absolute magnitudes. Photometric errors at U, B, V and K wavelengths are found to be 0.07, 0.02, 0.05 and 0.02 dex median values from Arnouts et al (2001), respectively.

fer significantly for galaxies inside the structures and the field. But the existence of what are likely to be more massive galaxies in the structures suggests that the specific star formation rate of galaxies in the structure are lower than that in the rest of the sample, implying that they are more evolved. This provides evidence that the evolution of galaxies in and around denser environments is faster than those in the field. In summary, the presence of large scale structures in the CDFS/GOODS-South field might also affect studies of the specific star formation and its evolution.

5. Conclusion

This paper prepares a series analysing the formation and evolution of intermediate massive galaxies at intermediate redshifts.

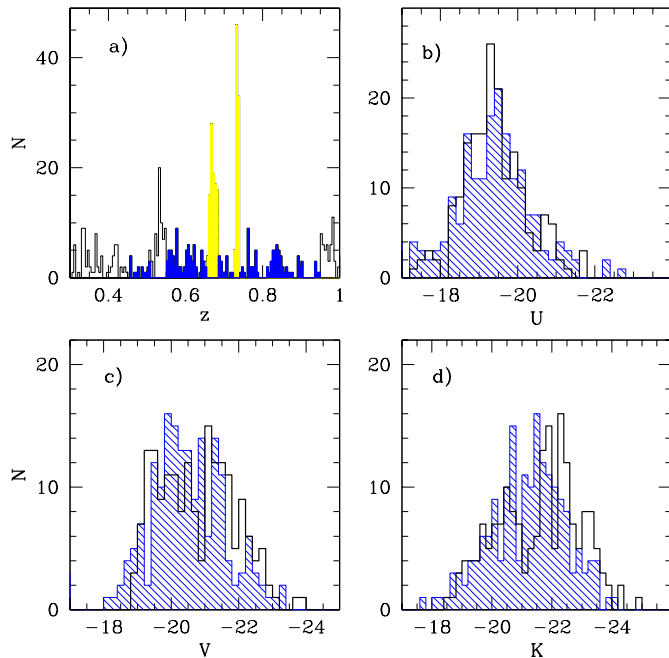


Fig. 13. Comparison of histograms of luminosities inside and outside the large scale structures present in CDFS. In Fig. **a**, the regions selected to represent the structure (yellow) and the field (blue) are shown. The redshift range for the galaxies in the two main structures is defined by 0.735 ± 0.009 and 0.668 ± 0.016 , while the field galaxies are taken from 0.7 ± 0.25 , excluding the structures mentioned above, and the smaller one at 0.530 ± 0.020 . In Fig. **b**, **c**, and **d** we show the distributions of U, V, K luminosities inside (open histogram) and outside (blue shaded) the structures.

Here we report the determination of new spectroscopic redshifts in the Chandra Deep Field South, using low-resolution VIMOS observations. We were able to spectroscopically identify 691 objects, consisting of 580 galaxies, 104 stars and seven QSOs. Employing an integration time of 45 minutes for two pointings with VIMOS, this study increases by 28% (and 35%) the availability of $I_{AB} \leq 23.5$ (and $I_{AB} \leq 22.5$) galaxies with redshift, which were poorly represented in the existing redshift surveys. The redshift distribution contains major peaks at 0.670, and 0.735, supporting the existence of large scale structures already detected by the VVDS and FORS2 surveys. The presence of large scale structures can arise various issues related to the cosmological variance of the GOODS. To analyse them, we construct a representative catalog of 640 galaxies with spectroscopic redshift with $I \leq 23.5$ and $z \leq 1$. Hence we attempt to analyse the “cosmological representativeness” of the GOODS region, by studying the properties of galaxies in GOODS in comparison with those of other surveys, including the CFRS. It results that the GOODS-South field is by far the most affected by the presence of large scale structures.

We do find a strong excess of luminosity density at $z=0.5-0.75$ in GOODS-South when compared to CFRS, especially in the V and K bands. This suggests that studies related to the evolution of the stellar mass and/or of the specific star formation

rate need to be interpreted cautiously. By analysing the galaxies inside and outside the structures in the GOODS field we find that the galaxies in the structure tend to be more massive and evolved compared to that outside the structures. This is likely at the origin of the luminosity density excess found in GOODS-South, at this redshift. Such an effect is found to be less prominent by using photometric redshifts instead of spectroscopic redshifts. However, on the sole basis of photometric redshifts in that field, it does not seem easy to disentangle effects related to galaxy evolution from those due the presence of large scale structures, because structures appear less prominent due to the uncertainties of the redshift determination. Spectroscopic redshifts are then highly essential for galaxy evolution studies.

The GOODS South field has been observed with an unprecedented depth at many wavelengths including optical and IR. It is one of the most studied cosmological fields, which has generated a large number of papers about the galaxy evolution. We stress out that many of these studies could be affected by cosmological variance of this field as revealed by our relatively modest spectroscopic study. We believe that this might affect some conclusions of studies based on photometric redshifts, especially those related to the evolution of stellar mass density and of specific star formation rate. Studies based on spectroscopic redshifts, such as IMAGES, have also to carefully compare the evolutionary properties of galaxies inside and outside the structures, before concluding about an overall picture of galaxy evolution.

Acknowledgements. CDR, AR and FH thank the Centre Franco-Indien pour la Promotion de la Recherche Avancee (CEFIPRA) for a post-doctoral fellowship and financial assistance respectively. We warmly thank our referee for his/her detailed comments and suggestions, which have contributed a lot in improving our manuscript.

References

- Appenzeller, I., Fricke, K., Furtig, W. et al. , 1998, The Messenger 94, 1
- Arnouts, S., Vandame, B., Benoist, C. et al. , 2001, A&A, 379, 740
- Bell, E. F. et al. 2003, ApJS, 149, 289
- Cimatti, A.; Mignoli, M., Daddi, E. et al. , 2002, A&A, 392, 395
- Crampton, D., Lilly, S., Le Fèvre, O., Hammer, F., 1995, ApJ 455, 96
- Elbaz, D., Cesarsky, C. J., Chanial, P. et al. , 2002, A&A, 384, 848
- Flores, H., Hammer, F., Puech, M., Amram, P., & Balkowski, C., 2006, A&A 455, 107
- Flores, H., Hammer, F., Thuan, T. et al. , 1999, ApJ, 517, 148
- Flores, H., Puech, M., Hammer, F., Garrido, O., & Hernandez, O., 2004, A&A, 420, 31
- Gilli, R., Cimatti, A., Daddi, E. et al. , 2003, ApJ, 592, 721
- Hammer, F., Gruel, N., Thuan, T. X., Flores, H. & Infante, L., 2001, A&A, 350, 570
- Hammer, F., Flores, H., Elbaz, D., et al. , 2005, A&A, 430, 115
- Heavens, A., Panter, B., Jimenez, R.,& Dunlop, J., 2004, Nature, 428, 625
- Le Fèvre, O., Vettolani, G., Garilli, B. et al. , 2005, A&A, 439, 845
- Le Fèvre, O., Vettolani, G., Paltani, S. et al. , 2004, A&A, 428, 1043
- Le Floc'h, E., Papovich, C., Dole, H. et al. , 2005, ApJ, 632, 169
- Mignoli, M., Cimatti, A., Zamorini, G. et al. , 2005, A&A, 437, 883
- Navarro, J. F., Frenk, C. S.& White, S. D. M., 1997, ApJ, 490, 493
- Puech, M., Hammer, F., Flores, H., Ostlin, G., & T. Marquart, 2006a, A&A 455, 119

- Puech, M., Flores, H., Hammer, F., & Lehnert, M.D., 2006b, A&A
455, 131
- Szokoly, G. P., Bergeron, J., Hasinger, G. et al. , 2004, ApJS, 155, 271
- Tully, R.B. & Fisher, J.R., 1977, A&A, 54, 651
- Vanzella, E., Cristiani, S., Dickinson, M. et al. , 2005, A&A, 434, 53
- Vanzella, E., Cristiani, S., Dickinson, M. et al. , 2006, A&A, 454, 423
- Wirth, G.D., Willmer, C., Amico, P., AJ, 2004, 127, 3121
- Wolf, C., Meisenheimer, K., Kleinheinrich, M. et al. , 2004, A&A,
421, 913
- Zheng, X. Z., Hammer, F., Flores, H., Assémat, F., Pelat, D., 2004,
A&A, 421, 847

Table 2. The redshift catalog of the 691 objects from the CDFS.

ID	T ^a	Q ^a	IntID ^b	z	I _{iso} ^c	M _U	M _B	M _V	M _J	M _K
EISJ033148.35-274816.6	2	1	1010003	0.843	22.66	-19.53	-20.38	-20.50	99.99	99.99
EISJ033135.20-274713.9	2	1	1010004	0.572	21.83	-18.71	-19.80	-20.58	99.99	99.99
EISJ033151.63-274823.9	1	1	1010006	0.677	20.81	-20.63	-21.50	-22.04	99.99	99.99
EISJ033138.49-274721.8	1	1	1010007	0.549	23.10	-18.01	-18.76	-19.01	99.99	99.99
EISJ033152.87-274824.4	1	2	1010009	0.685	21.69	-19.16	-20.53	-21.46	99.99	99.99
EISJ033133.92-274641.5	3	1	1010013	1.060	21.47	-21.79	-22.75	-23.26	99.99	99.99
EISJ033149.68-274751.7	1	1	1010014	0.184	21.55	-16.15	-17.06	-17.71	99.99	99.99
EISJ033200.70-274839.2	2	1	1010015	0.534	21.88	-19.10	-19.88	-20.17	99.99	99.99
EISJ033145.60-274718.9	1	1	1010016	0.602	23.11	-16.54	-18.62	-19.55	99.99	99.99
EISJ033132.92-274622.8	1	1	1010017	0.738	22.98	-18.84	-19.64	-20.03	99.99	99.99
EISJ033201.94-274832.1	1	1	1010018	0.777	22.27	-20.02	-20.53	-20.62	99.99	99.99
EISJ033147.54-274721.8	1	2	1010019	0.525	23.01	-18.07	-18.71	-19.00	99.99	99.99
EISJ033132.46-274610.2	3	1	1010020	0.743	22.79	-18.73	-19.83	-20.38	99.99	99.99
EISJ033203.13-274817.5	3	1	1010021	0.295	19.85	-17.97	-19.60	-20.54	99.99	99.99
EISJ033143.66-274645.4	1	1	1010022	0.476	21.36	-18.46	-19.66	-20.47	99.99	99.99
EISJ033137.50-274545.6	3	1	1010029	1.071	22.41	-20.26	-22.35	-23.29	99.99	99.99
EISJ033205.67-274749.5	2	1	1010032	0.899	23.02	-19.53	-20.29	-20.49	99.99	99.99
EISJ033135.82-274522.8	3	1	1010034	0.815	21.60	-20.75	-21.34	-21.49	99.99	99.99
EISJ033152.85-274636.3	1	1	1010035	0.677	22.65	-19.28	-19.81	-19.90	99.99	99.99
EISJ033206.41-274735.2	2	1	1010037	0.557	24.25	-17.16	-17.71	-17.86	99.99	99.99
EISJ033144.84-274551.7	1	2	1010038	0.735	20.42	-20.49	-22.09	-23.02	99.99	99.99
EISJ033155.28-274635.1	2	1	1010040	0.949	22.39	-19.93	-21.45	-22.21	99.99	99.99
EISJ033137.25-274508.6	1	1	1010041	1.030	23.40	-19.92	-20.56	-20.89	99.99	99.99
EISJ033204.76-274715.8	2	1	1010042	1.273	21.73	-22.47	-22.98	-23.07	99.99	99.99
EISJ033139.06-274511.6	2	1	1010044	0.744	22.68	-19.03	-19.96	-20.40	99.99	99.99
EISJ033205.31-274700.1	3	1	1010045	0.974	23.04	-19.65	-20.93	-21.66	99.99	99.99
EISJ033148.98-274540.2	1	1	1010046	0.419	22.10	-17.79	-18.66	-19.34	99.99	99.99
EISJ033137.32-274441.9	1	1	1010047	0.707	21.13	-19.35	-21.21	-22.14	99.99	99.99
EISJ033159.09-274619.3	1	1	1010048	0.671	23.09	-18.86	-19.34	-19.46	99.99	99.99
EISJ033140.79-274452.4	2	1	1010049	0.685	22.69	-18.41	-19.61	-20.30	99.99	99.99
EISJ033141.32-274448.0	2	1	1010050	0.687	22.49	-18.75	-19.87	-20.42	99.99	99.99
EISJ033155.08-274547.3	1	1	1010052	0.096	21.08	-17.16	-17.23	-17.06	99.99	99.99
EISJ033145.25-274447.2	2	2	1010054	0.939	22.68	-19.95	-21.05	-21.75	99.99	99.99
EISJ033204.79-274614.7	2	3	1010055	1.390	22.67	-22.28	-23.19	-23.87	-24.48	-24.45
EISJ033152.13-274510.4	1	2	1010056	0.530	21.05	-18.29	-20.22	-21.16	99.99	99.99
EISJ033157.18-274524.4	1	3	1010058	1.237	23.67	-20.26	-20.36	-20.22	99.99	99.99
EISJ033205.98-274601.6	2	2	1010060	0.535	20.81	-18.79	-20.50	-21.43	-22.28	-22.26
EISJ033208.26-274602.8	3	1	1010063	1.086	24.44	-18.95	-19.67	-19.87	-20.25	-20.14
EISJ033142.82-274400.6	3	1	1010064	1.020	22.48	-20.86	-21.35	-21.55	99.99	99.99
EISJ033206.86-274550.2	1	1	1010065	0.848	21.53	-20.91	-21.56	-21.81	-21.91	-21.81
EISJ033139.60-274339.5	2	1	1010067	0.958	22.49	-20.05	-21.57	-22.49	99.99	99.99
EISJ033200.56-274501.5	1	2	1010068	0.573	20.72	-18.80	-20.83	-21.76	99.99	99.99
EISJ033140.39-274325.9	2	1	1010069	0.335	21.64	-18.08	-18.72	-19.20	99.99	99.99
EISJ033144.59-274338.9	1	1	1010070	1.030	22.16	-21.10	-21.77	-22.06	99.99	99.99
EISJ033155.64-274400.3	2	2	1010077	0.689	21.76	-18.78	-20.48	-21.42	99.99	99.99
EISJ033144.06-274305.6	1	1	1010078	0.734	22.96	-18.73	-19.61	-20.19	99.99	99.99
EISJ033149.71-274326.6	2	1	1010080	0.623	20.02	-20.51	-21.85	-22.76	99.99	99.99
EISJ033149.55-274319.6	1	3	1010082	1.320	21.74	-22.71	-23.47	-23.88	99.99	99.99
EISJ033205.42-274429.4	2	1	1010083	0.667	23.65	-17.92	-18.71	-19.00	-20.05	-19.97
EISJ033158.23-274349.3	1	1	1010084	0.334	21.97	-17.64	-18.41	-18.86	99.99	99.99
EISJ033200.83-274354.3	2	2	1010086	0.917	23.14	55.51	-20.64	-21.57	99.99	99.99
EISJ033141.53-274222.0	2	1	1010087	0.523	19.26	-21.51	-22.21	-22.82	99.99	99.99
EISJ033159.26-274341.6	1	1	1010088	0.183	22.32	-15.51	-16.38	-16.96	-17.14	-17.06
EISJ033148.76-274250.3	1	1	1010089	0.949	21.28	-20.33	-22.72	-23.66	99.99	99.99
EISJ033155.19-274315.7	1	1	1010090	0.486	21.92	-17.64	-19.08	-20.00	99.99	99.99
EISJ033200.56-274332.8	1	1	1010092	0.444	22.13	-18.13	-18.92	-19.47	-19.29	-19.19
EISJ033150.32-274241.1	1	2	1010093	0.622	21.61	-18.06	-20.24	-21.17	99.99	99.99
EISJ033139.99-274157.3	1	1	1010094	0.468	19.27	-21.31	-21.67	-22.51	99.99	99.99
EISJ033147.76-274211.1	3	1	1010100	1.070	23.25	-20.30	-20.72	-20.81	99.99	99.99
EISJ033206.91-274337.0	1	1	1010101	0.676	22.47	-18.79	-19.84	-20.37	-20.56	-20.46
EISJ033152.47-274228.1	1	2	1010102	0.734	21.13	-18.82	-21.37	-22.31	99.99	99.99
EISJ033212.37-274353.8	3	1	1010104	0.944	20.98	-21.80	-22.65	-23.13	-23.66	-23.62
EISJ033204.04-274308.5	1	2	1010106	0.604	20.90	-19.41	-20.84	-21.78	-22.56	-22.52
EISJ033159.84-274241.2	3	1	1010108	0.821	22.67	-19.37	-20.36	-21.01	-21.59	-21.50
EISJ033200.93-274241.2	1	2	1010109	0.540	20.19	-19.61	-21.15	-22.08	-23.33	-23.30
EISJ033205.14-274253.2	1	1	1010111	0.549	21.90	-18.28	-19.54	-20.41	-21.48	-21.46
EISJ033155.42-274207.9	2	1	1010112	0.681	20.10	-20.31	-22.09	-23.03	99.99	99.99
EISJ033141.86-274059.8	2	2	1010113	0.570	21.55	-18.28	-19.98	-20.91	99.99	99.99
EISJ033206.73-274524.3	1	1	1010114	0.848	22.51	-19.97	-20.53	-20.55	-20.50	-20.28
EISJ033210.88-274438.9	1	1	1010116	0.729	22.44	-19.83	-20.22	-20.21	-20.53	-20.43
EISJ033209.56-274356.0	1	2	1010117	0.478	21.26	-18.71	-19.82	-20.58	-21.11	-21.04
EISJ033210.97-274330.0	3	1	1010118	1.123	22.81	-20.78	-21.74	-22.30	-22.70	-22.62
EISJ033208.69-274508.2	2	1	1010120	0.783	23.50	-17.67	-19.32	-20.06	-22.26	-22.24
EISJ033209.78-274442.6	1	1	1010121	0.083	18.28	-16.46	-17.92	-18.85	-19.85	-19.83
EISJ033158.69-274500.6	2	2	1010122	0.575	20.28	-20.19	-21.30	-22.20	99.99	99.99
EISJ033154.17-274223.5	2	1	1010123	0.931	22.87	-19.80	-20.77	-21.38	99.99	99.99
EISJ033202.65-274828.2	1	2	1010131	0.946	23.07	-19.70	-20.65	-21.26	99.99	99.99
EISJ033206.08-274645.4	1	1	1010134	0.622	21.79	-19.58	-20.34	-20.72	99.99	99.99
EISJ033203.74-274748.3	1	2	1010136	0.670	22.40	-17.96	-19.73	-20.66	99.99	99.99
EISJ033203.49-274731.5	2	1	1010137	1.159	24.08	-19.76	-20.42	-20.71	99.99	99.99
GASJ033140.18-274235.1	2	1	1010139	0.570	99.99	57.93	57.80	57.94	99.99	99.99
EISJ033147.50-275738.3	1	1	1021001	0.245	22.93	-16.54	-17.07	-17.22	99.99	99.99
EISJ033134.88-275633.7	2	1	1021002	0.206	99.99	60.59	60.17	60.17	99.99	99.99
EISJ033214.98-275625.2	1	2	1020002	0.821	20.45	21.68	22.42	21.37	99.99	99.99

Table 2. Cont...

ID	T ^a	Q ^a	IntID ^b	z	I _{ISD} ^c	M _U	M _B	M _V	M _J	M _K
EISJ033125.51-275518.1	2	1	1020012	0.744	21.47	56.86	-21.10	-22.03	99.99	99.99
EISJ033130.14-275528.6	1	1	1020014	0.104	19.50	-17.22	-17.99	-18.46	99.99	99.99
EISJ033145.57-275526.0	1	1	1020018	0.698	21.57	-20.14	-20.88	-21.29	99.99	99.99
EISJ033130.28-275505.2	1	1	1020020	0.111	20.71	-16.11	-16.93	-17.41	99.99	99.99
EISJ033148.79-275526.3	1	1	1020021	0.731	22.12	-20.14	-20.54	-20.57	99.99	99.99
EISJ033119.75-275406.4	1	1	1020022	0.776	22.71	-19.08	-20.07	-20.77	99.99	99.99
EISJ033151.24-275635.1	2	1	1020023	0.696	20.88	-20.40	-21.46	-22.19	99.99	99.99
EISJ033129.60-275434.2	2	1	1020027	0.548	21.90	-18.78	-19.71	-20.32	99.99	99.99
EISJ033144.74-275543.7	1	1	1021028	0.780	23.26	-19.29	-19.55	-19.67	99.99	99.99
EISJ033144.81-275542.3	1	1	1022028	0.777	22.83	-18.86	-19.96	-20.44	99.99	99.99
EISJ033138.09-275453.6	2	1	1020029	0.672	22.65	-18.59	-19.61	-20.22	99.99	99.99
EISJ033125.93-275352.4	1	1	1020030	1.105	23.13	-20.20	-21.85	-22.77	99.99	99.99
EISJ033145.11-275520.7	2	1	1020031	1.235	21.10	-23.04	-24.12	-24.83	99.99	99.99
EISJ033145.30-275511.8	2	1	1020033	0.603	21.59	-18.50	-20.14	-21.08	99.99	99.99
GASJ033124.02-275455.8	1	1	1020034	0.259	99.99	60.07	59.65	59.65	99.99	99.99
EISJ033151.10-275529.2	1	1	1020035	0.217	19.64	-17.63	-18.98	-19.91	99.99	99.99
EISJ033128.50-275342.1	1	1	1020037	0.267	19.06	-18.63	-20.11	-21.05	99.99	99.99
EISJ033141.26-275435.0	1	1	1020038	0.334	20.31	-18.76	-19.81	-20.49	99.99	99.99
EISJ033129.04-275335.5	1	1	1020039	0.292	22.89	-15.90	-16.84	-17.54	99.99	99.99
EISJ033142.76-275431.6	3	1	1020041	0.723	22.98	-19.44	-19.67	-19.61	99.99	99.99
EISJ033128.62-275323.7	2	1	1020042	0.128	19.74	-17.29	-18.15	-18.69	99.99	99.99
EISJ033150.62-275502.0	1	2	1020043	0.737	22.85	-17.47	-19.67	-20.60	99.99	99.99
EISJ033141.59-275356.2	2	1	1020047	0.357	22.52	-15.67	-17.50	-18.43	99.99	99.99
EISJ033131.07-275302.6	2	2	1020048	0.589	21.75	-19.42	-20.20	-20.61	99.99	99.99
EISJ033154.39-275449.4	2	2	1020049	0.532	22.30	-17.06	-18.99	-19.92	99.99	99.99
EISJ033142.80-275350.9	2	1	1020050	0.934	22.91	-20.13	-20.47	-20.49	99.99	99.99
EISJ033129.53-275247.3	3	1	1020051	1.026	20.20	-21.70	-23.81	-24.26	99.99	99.99
EISJ033153.75-275433.8	1	1	1020052	0.670	22.64	-17.94	-19.49	-20.42	99.99	99.99
EISJ033141.16-275336.4	2	2	1020053	0.499	21.03	-18.15	-20.05	-20.98	99.99	99.99
EISJ033126.12-275212.4	1	2	1020057	0.486	22.69	59.08	-18.30	-19.23	99.99	99.99
EISJ033153.74-275422.3	1	1	1020058	0.731	20.87	-20.67	-21.68	-22.32	99.99	99.99
EISJ033146.35-275324.9	2	1	1020061	0.929	22.04	-19.52	-21.83	-22.76	99.99	99.99
EISJ033132.80-275218.6	1	1	1020062	0.595	19.77	-20.69	-21.94	-22.83	99.99	99.99
EISJ033155.62-275402.3	3	1	1020063	0.052	22.75	-12.60	-13.30	-13.69	99.99	99.99
EISJ033126.49-275142.3	3	1	1020064	1.370	23.05	-21.53	-22.68	-23.33	99.99	99.99
EISJ033124.41-275122.3	1	1	1020066	0.333	21.16	-18.16	-19.10	-19.65	99.99	99.99
EISJ033148.39-275314.4	2	2	1020067	0.528	21.45	-17.71	-19.81	-20.75	99.99	99.99
EISJ033135.88-275212.0	1	1	1020068	0.381	20.96	-18.76	-19.64	-20.21	99.99	99.99
EISJ033149.02-275309.6	1	1	1020070	0.958	22.30	-20.71	-21.33	-21.67	99.99	99.99
EISJ033131.30-275144.2	1	1	1020071	0.751	19.81	-22.10	-22.86	-23.31	99.99	99.99
EISJ033125.27-275107.1	2	1	1020073	0.583	21.54	-19.29	-20.26	-20.87	99.99	99.99
EISJ033127.80-275114.3	1	1	1020075	0.587	20.91	-19.38	-20.73	-21.65	99.99	99.99
EISJ033129.11-275114.3	1	1	1020077	0.681	21.06	-19.97	-21.19	-21.95	99.99	99.99
EISJ033150.33-275250.1	1	1	1020078	0.696	21.61	-18.69	-20.67	-21.60	99.99	99.99
EISJ033128.07-275100.9	3	1	1020080	1.016	22.55	-20.54	-21.37	-21.75	99.99	99.99
EISJ033156.62-275309.9	1	1	1020081	0.248	19.98	-17.92	-19.13	-19.97	99.99	99.99
EISJ033152.18-275242.4	1	1	1020084	0.646	21.26	-19.52	-20.77	-21.62	99.99	99.99
EISJ033154.58-275246.3	1	1	1020086	0.772	22.10	-20.09	-20.68	-20.83	99.99	99.99
EISJ033139.22-275133.0	2	1	1020087	0.972	21.86	-19.61	-22.30	-23.24	99.99	99.99
EISJ033136.31-275102.6	1	1	1020088	0.414	21.11	-19.06	-19.81	-20.29	99.99	99.99
EISJ033155.64-275224.1	3	1	1020091	0.822	21.97	-20.31	-21.03	-21.38	99.99	99.99
EISJ033132.81-275031.9	1	1	1020092	0.746	22.88	-19.18	-19.80	-20.00	99.99	99.99
EISJ033149.39-275140.2	2	2	1020095	0.669	21.61	-19.31	-20.56	-21.37	99.99	99.99
EISJ033130.02-274950.8	1	1	1020097	0.845	22.31	-20.22	-20.75	-20.90	99.99	99.99
EISJ033130.06-274946.0	1	1	1020098	0.362	21.91	-17.84	-18.61	-19.13	99.99	99.99
EISJ033140.85-275032.2	1	1	1020100	0.554	22.57	-18.30	-19.18	-19.63	99.99	99.99
EISJ033155.26-275136.5	1	1	1020102	0.562	21.73	-19.00	-20.10	-20.49	99.99	99.99
EISJ033142.51-275033.3	1	1	1020103	0.093	18.76	-18.24	-18.93	-19.12	99.99	99.99
EISJ033152.81-275115.6	2	2	1020105	0.561	21.78	-17.31	-19.69	-20.62	99.99	99.99
EISJ033128.09-275040.2	2	2	1020112	0.464	23.23	-17.19	-17.86	-18.50	99.99	99.99
EISJ033150.43-275212.3	1	1	1020116	0.238	23.48	-13.70	-15.38	-16.32	99.99	99.99
EISJ033141.13-275046.2	2	1	1020118	0.562	22.51	-17.27	-18.96	-19.90	99.99	99.99
EISJ033123.20-275145.5	2	1	1020120	0.498	19.33	-18.78	-21.90	-22.63	99.99	99.99
EISJ033119.54-275400.8	1	2	1020121	0.569	21.52	-17.89	-20.00	-20.93	99.99	99.99
EISJ033119.54-275416.9	3	1	1020122	1.034	23.69	-19.62	-20.20	-20.40	99.99	99.99
EISJ033122.98-275345.4	3	1	1020123	1.068	22.97	54.49	-21.78	-22.71	99.99	99.99
EISJ033130.25-275459.7	2	1	1020124	0.341	23.11	-16.98	-17.51	-17.80	99.99	99.99
EISJ033142.24-275353.9	2	1	1020128	0.763	25.25	-17.43	-17.51	-17.45	99.99	99.99
EISJ033148.81-275350.6	1	1	1020133	0.212	24.03	-15.62	-15.88	-15.86	99.99	99.99
EISJ033226.59-280112.6	2	2	1030001	0.617	20.41	-20.98	-21.71	-22.06	99.99	99.99
EISJ033222.75-280043.6	3	1	1030003	0.182	20.74	-16.00	-17.42	-18.35	99.99	99.99
EISJ033213.21-275952.9	2	1	1030004	0.446	20.49	-19.72	-20.59	-21.12	99.99	99.99
EISJ033228.99-280059.5	2	1	1030006	0.282	21.06	-15.29	-18.27	-19.20	99.99	99.99
EISJ033213.16-275944.4	2	2	1030007	0.537	21.70	-18.50	-19.73	-20.50	99.99	99.99
EISJ033210.84-275927.0	2	1	1030009	0.651	19.59	-20.16	-22.43	-23.37	99.99	99.99
EISJ033209.31-275912.8	1	1	1030011	0.452	20.69	-19.39	-20.35	-20.96	99.99	99.99
EISJ033209.30-275907.3	2	2	1030013	0.450	19.82	-20.32	-21.26	-21.82	99.99	99.99
EISJ033219.08-275946.9	1	1	1030015	0.735	22.60	-19.48	-20.05	-20.21	99.99	99.99
EISJ033207.97-275853.5	1	1	1030016	0.214	21.52	-17.11	-17.80	-18.20	99.99	99.99
EISJ033228.82-275851.6	2	1	1030018	0.950	20.75	-21.95	-23.26	-24.19	99.99	99.99
EISJ033233.15-280041.4	1	2	1030019	0.674	20.88	-19.23	-21.27	-22.21	99.99	99.99
EISJ033222.27-275949.8	1	1	1030020	0.214	21.24	-17.07	-17.90	-18.44	99.99	99.99
EISJ033227.29-280002.6	1	2	1030022	0.597	22.57	-16.79	-19.13	-20.06	99.99	99.99
EISJ033228.82-275951.6	2	1	1030025	0.784	21.33	56.54	-21.50	-22.43	99.99	99.99

Table 2. Cont...

ID	T ^a	Q ^a	IntID ^b	z	I _{iso} ^c	M _U	M _B	M _V	M _J	M _K
EISJ033225.01-275833.5	2	2	1030037	0.538	21.51	58.54	-19.82	-20.75	99.99	99.99
EISJ033228.78-275844.8	3	1	1030039	0.176	21.93	-14.69	-16.14	-17.08	99.99	99.99
EISJ033206.52-275659.1	1	1	1030041	0.661	21.09	-20.00	-21.08	-21.78	99.99	99.99
EISJ033235.00-275904.6	2	1	1030042	0.087	21.03	-13.80	-15.28	-16.21	99.99	99.99
EISJ033225.13-275818.3	3	1	1030043	0.782	17.92	-24.17	-24.90	-25.83	99.99	99.99
EISJ033209.41-275659.1	2	2	1030045	0.594	21.88	-18.86	-19.91	-20.64	99.99	99.99
EISJ033206.85-275640.4	2	1	1030046	0.219	19.20	-17.74	-19.44	-20.37	99.99	99.99
EISJ033223.35-275752.6	2	1	1030048	0.681	18.86	57.23	-23.33	-24.27	99.99	99.99
EISJ033207.77-275638.3	2	2	1030049	0.619	21.57	-18.02	-20.26	-21.20	99.99	99.99
EISJ033228.42-275810.3	1	1	1030050	0.217	18.71	-18.46	-19.91	-20.84	99.99	99.99
EISJ033218.91-275726.4	1	1	1030051	0.121	21.56	-14.73	-15.85	-16.61	99.99	99.99
EISJ033232.39-275820.2	1	1	1030053	0.288	22.85	-17.56	-17.75	-17.73	99.99	99.99
EISJ033223.01-275732.1	1	1	1030054	0.734	20.45	-22.48	-22.13	-22.67	99.99	99.99
EISJ033213.03-275647.5	1	1	1030055	0.369	21.65	-17.87	-18.73	-19.43	99.99	99.99
EISJ033235.30-275824.5	3	1	1030056	1.370	22.64	-22.04	-22.96	-23.54	99.99	99.99
EISJ033223.08-275727.5	1	1	1030057	0.684	20.93	57.21	-21.28	-22.21	99.99	99.99
EISJ033206.98-275610.4	1	1	1030058	0.777	20.88	-20.88	-21.91	-22.55	99.99	99.99
EISJ03230.61-275756.9	3	1	1030059	0.116	23.51	-14.54	-14.95	-14.98	99.99	99.99
EISJ033224.57-275723.0	1	1	1030061	0.202	22.57	-16.43	-16.91	-17.11	99.99	99.99
EISJ033209.16-275608.3	1	2	1030062	0.740	22.65	-19.42	-20.01	-20.21	99.99	99.99
EISJ033235.08-275803.3	1	1	1030063	0.219	21.91	-16.44	-17.23	-17.81	99.99	99.99
EISJ033221.74-275702.2	3	1	1030064	0.953	21.74	-21.17	-22.08	-22.79	99.99	99.99
EISJ033211.34-275609.8	1	1	1030065	0.617	22.34	-19.13	-19.81	-20.10	99.99	99.99
EISJ033210.78-275601.2	1	1	1030067	0.594	19.74	-20.86	-21.99	-22.83	99.99	99.99
EISJ033226.83-275710.2	1	1	1030069	0.278	23.09	-15.11	-16.30	-17.16	99.99	99.99
EISJ033217.17-275626.2	1	1	1030070	0.776	21.88	-20.01	-20.90	-21.51	99.99	99.99
EISJ033233.69-275724.5	1	1	1030072	0.634	23.45	-17.57	-18.61	-19.26	99.99	99.99
EISJ033215.49-275555.6	2	2	1030073	0.966	21.71	-20.34	-22.41	-23.34	99.99	99.99
EISJ033231.78-275708.1	2	2	1030074	0.492	23.08	-16.33	-17.95	-18.88	99.99	99.99
EISJ033217.82-275601.3	1	1	1030075	0.675	22.67	-19.28	-19.77	-19.89	-20.24	-20.07
EISJ033235.07-275712.7	1	1	1030077	0.667	22.66	-18.89	-19.65	-20.06	99.99	99.99
EISJ033213.23-275528.8	3	1	1030079	1.105	21.50	-21.42	-23.50	-24.44	99.99	99.99
EISJ033222.24-275604.9	2	2	1030080	0.487	20.23	-19.18	-20.76	-21.70	-22.66	-22.63
EISJ033210.14-275507.2	2	2	1030081	1.127	21.73	-20.31	-23.42	-24.36	99.99	99.99
EISJ033217.99-275529.4	1	1	1030085	0.826	23.02	-19.39	-19.96	-20.08	-20.75	-20.56
EISJ033223.19-275541.2	1	1	1030087	0.735	22.78	-19.26	-19.86	-20.06	-20.55	-20.44
EISJ033214.85-275456.2	2	1	1030089	0.280	21.96	-15.77	-17.35	-18.28	99.99	99.99
EISJ033223.77-275528.5	2	1	1030091	0.510	22.17	-19.43	-19.74	-19.68	-19.80	-19.53
EISJ033208.08-275414.1	2	1	1030092	0.682	21.61	-19.57	-20.65	-21.40	99.99	99.99
EISJ033231.18-275557.3	1	1	1030093	0.841	23.74	-18.76	-19.29	-19.35	-19.25	-18.86
EISJ033210.23-275416.4	1	2	1030094	0.765	22.63	-18.26	-20.07	-21.00	99.99	99.99
EISJ033228.07-275526.7	1	1	1030097	0.665	20.33	-19.58	-21.77	-22.70	-23.57	-23.51
EISJ033216.56-275429.3	1	1	1030098	0.662	21.63	-18.84	-20.45	-21.39	-22.30	-22.27
EISJ033234.88-275547.7	2	1	1030099	0.346	22.04	-16.69	-17.97	-18.83	-19.28	-19.15
EISJ033223.03-275452.4	1	1	1030100	0.659	20.96	-20.59	-21.35	-21.68	-22.38	-22.30
EISJ033211.81-275357.3	1	1	1030101	0.665	21.02	-19.94	-21.14	-21.91	99.99	99.99
EISJ033223.24-275445.9	1	1	1030103	0.403	21.79	-18.30	-19.02	-19.54	-19.95	-19.81
EISJ033210.63-275342.8	2	1	1030104	1.097	20.98	-22.49	-23.33	-23.74	99.99	99.99
EISJ033235.09-275533.1	3	1	1030105	0.039	15.71	-16.90	-18.73	-19.66	-21.22	-21.19
EISJ033224.54-275443.0	1	1	1030106	0.125	18.94	-16.81	-18.26	-19.19	-20.41	-20.39
EISJ033210.71-275336.9	1	1	1030107	1.068	22.33	-20.83	-22.00	-22.62	99.99	99.99
EISJ033227.73-275451.8	2	1	1030108	1.075	22.51	-20.97	-21.75	-22.23	-22.26	-22.16
EISJ033231.30-275456.0	1	1	1030111	0.656	23.91	-17.59	-18.42	-18.66	-19.07	-18.91
EISJ033209.79-275313.1	1	1	1030113	0.743	21.86	-19.28	-20.70	-21.60	99.99	99.99
EISJ033235.09-275505.0	2	2	1030114	0.502	21.77	-19.08	-19.76	-20.15	-20.38	-20.28
EISJ033221.91-275403.2	2	2	1030115	1.003	23.47	-19.39	-20.50	-21.08	-21.64	-21.56
EISJ033227.37-275421.5	1	1	1030116	0.653	21.87	-19.51	-20.39	-20.78	-21.45	-21.37
EISJ033210.94-275754.7	1	1	1030120	0.043	20.32	-15.05	-15.63	-15.83	99.99	99.99
EISJ033212.36-275257.3	1	1	1030128	0.731	22.67	-19.35	-19.96	-20.16	99.99	99.99
EISJ033238.04-275508.3	1	1	1030129	0.372	21.33	-18.14	-19.09	-19.77	-20.10	-19.95
EISJ033215.82-275324.7	2	2	1030131	0.676	22.13	-18.75	-20.06	-20.92	-22.12	-22.08
EISJ033223.15-275426.0	1	3	1030133	1.519	20.99	-24.22	-25.30	-25.95	-24.63	-24.53
EISJ033240.39-275548.3	1	1	1030134	0.127	23.52	-15.69	-15.59	-15.36	-15.44	-15.22
EISJ033231.96-275553.5	1	1	1030135	0.839	22.96	-19.50	-20.06	-20.15	-20.84	-20.68
EISJ033231.09-275612.6	1	2	1030136	0.667	21.29	-19.11	-20.82	-21.76	-22.35	-22.29
EISJ033239.70-275507.3	1	1	1030137	0.366	21.09	-18.46	-19.36	-19.97	-20.43	-20.34
EISJ033233.04-275938.7	3	1	1030140	1.014	22.98	-20.16	-21.00	-21.49	99.99	99.99
EISJ033215.55-275801.9	1	1	1030144	0.738	21.34	-20.55	-21.29	-21.65	99.99	99.99
EISJ033235.38-280005.3	1	1	1030153	0.128	18.83	-17.34	-18.56	-19.42	99.99	99.99
EISJ033237.50-275216.2	2	1	1040001	0.583	20.90	-20.43	-21.09	-21.38	-21.66	-21.57
EISJ033221.15-275102.3	2	1	1040002	1.274	22.79	-21.52	-22.39	-22.93	-22.72	-22.63
EISJ033225.96-275058.9	2	1	1040005	0.669	23.84	-17.50	-18.46	-18.92	-20.63	-20.57
GASJ033220.70-275022.2	2	1	1040010	0.735	23.88	-18.24	-18.79	-18.85	-19.56	-19.30
EISJ033232.14-275105.7	1	1	1040011	0.683	22.17	-18.57	-20.07	-20.89	-21.70	-21.65
EISJ033236.39-275117.8	1	1	1040012	0.268	20.52	-17.48	-18.76	-19.62	-20.23	-20.14
EISJ033239.33-275117.4	1	1	1040015	0.691	23.05	-19.19	-19.50	-19.43	-19.58	-19.49
EISJ033227.37-275015.9	1	1	1040018	0.771	21.89	-20.20	-20.88	-21.17	-22.00	-21.90
EISJ033218.93-274929.4	1	1	1040021	0.331	23.54	-16.92	-17.25	-17.33	-18.13	-17.93
EISJ033217.84-274915.9	3	1	1040022	1.127	23.77	-19.93	-20.18	-20.11	-20.35	-20.14
EISJ033241.78-275101.0	1	2	1040024	0.579	21.76	-17.87	-18.92	-19.82	-20.76	-21.60
EISJ033242.28-275056.5	1	1	1040026	0.577	23.29	-18.09	-18.65	-18.98	-19.49	-19.39
EISJ033231.59-275004.7	1	1	1040027	0.532	21.79	-18.72	-19.68	-20.36	-20.92	-20.83
EISJ033249.71-275125.9	3	1	1040028	0.271	23.45	-16.10	-16.66	-16.91	-17.61	-17.38
EISJ033238.37-275029.0	1	1	1040029	0.601	21.72	-19.28	-20.20	-20.77	-21.28	-21.19

Table 2. Cont...

ID	T ^a	Q ^a	IntID ^b	z	I _{iso} ^c	M _U	M _B	M _V	M _J	M _K
EISJ033224.62-274851.5	2	1	1040037	0.676	20.82	-20.72	-21.48	-22.03	-22.73	-22.65
EISJ033220.35-274819.8	2	1	1040038	0.577	23.95	-17.87	-18.16	-18.20	-20.11	-20.02
EISJ033236.20-274932.0	1	1	1040040	0.549	20.41	-19.51	-20.99	-21.92	-23.00	-22.98
EISJ033227.39-274842.3	1	1	1040042	0.672	23.31	-18.74	-19.17	-19.15	-19.41	-19.03
EISJ033232.74-274859.6	1	1	1040043	0.670	21.94	-19.41	-20.33	-20.89	-21.55	-21.46
EISJ033221.12-274744.4	2	1	1040045	0.671	23.03	-18.82	-19.40	-19.52	-19.80	-19.64
EISJ033244.72-274923.0	1	1	1040046	0.574	21.33	-19.23	-20.35	-21.07	-21.53	-21.45
EISJ033219.88-274721.4	1	2	1040048	0.733	21.68	-18.81	-20.82	-21.75	-22.54	-22.50
EISJ033251.74-274951.3	1	1	1040049	0.736	21.27	-20.53	-21.33	-21.81	-22.42	-22.33
EISJ033220.66-274717.0	1	1	1040051	0.735	21.28	-20.51	-21.32	-21.79	-22.31	-22.22
EISJ033246.38-274913.1	1	2	1040052	0.681	22.18	-18.08	-20.01	-20.95	-21.89	-21.84
EISJ033224.36-274725.1	2	2	1040053	0.527	22.10	-18.08	-19.27	-20.04	-20.68	-20.59
EISJ033235.99-274812.0	1	2	1040054	0.603	21.44	-18.86	-20.29	-21.23	-21.82	-21.73
EISJ033226.31-274717.6	2	1	1040057	0.133	22.32	-13.51	-15.04	-15.97	-17.21	-17.19
EISJ033239.24-274758.6	1	2	1040060	0.665	20.80	-19.30	-21.30	-22.23	-23.13	-23.08
EISJ033229.69-274710.4	2	1	1040061	0.690	23.89	-17.59	-18.52	-18.95	-20.25	-20.21
EISJ033241.96-274757.7	1	1	1040063	0.152	20.25	-17.39	-18.18	-18.63	-18.81	-18.65
EISJ03253.25-274833.8	1	1	1040065	0.225	20.61	-17.58	-18.55	-19.17	-19.20	-19.01
EISJ033240.34-274723.0	1	1	1040067	0.619	23.65	-18.05	-18.59	-18.71	-19.62	-19.53
EISJ033239.90-274715.2	1	3	1040069	1.112	21.79	-21.90	-22.66	-23.16	-23.14	-23.06
EISJ033228.76-274620.5	1	1	1040070	0.736	21.24	-19.56	-21.27	-22.21	-23.02	-22.97
EISJ033225.67-274555.6	1	1	1040072	1.040	23.58	-19.73	-20.10	-20.04	-20.54	-20.23
EISJ033243.59-274717.0	1	1	1040073	0.213	23.80	-16.53	-16.37	-16.17	-15.94	-15.38
EISJ033235.64-274633.0	2	1	1040074	0.564	23.02	-18.07	-18.81	-19.22	-20.20	-20.12
GASJ033236.43-274631.5	2	1	1041076	0.765	22.93	-19.28	-19.82	-19.98	-21.52	-21.43
GASJ033236.50-274629.3	2	1	1042076	0.764	21.53	-20.62	-21.22	-21.37	-22.04	-21.95
EISJ033238.61-274631.6	1	1	1040077	0.618	21.94	-19.44	-20.03	-20.68	-21.54	-21.45
EISJ033227.75-274518.9	1	1	1040082	0.683	23.91	-18.12	-18.57	-18.66	-19.46	-19.23
EISJ033230.07-274523.7	3	1	1040084	0.954	21.84	-20.91	-21.86	-22.38	-22.93	-22.85
EISJ033229.33-275155.4	2	1	1040098	0.511	22.65	-18.70	-19.17	-19.24	-19.50	-19.34
EISJ033217.58-274941.1	1	1	1040102	0.338	22.29	-17.80	-18.36	-18.61	-18.57	-18.31
EISJ033216.17-274941.8	1	2	1040103	0.663	20.35	-19.86	-21.74	-22.67	-23.60	-23.57
EISJ033243.64-275122.6	1	1	1040104	0.567	23.08	-18.41	-18.94	-19.06	-19.43	-19.17
EISJ033218.75-274834.2	1	1	1040108	0.290	22.02	-17.38	-18.12	-18.47	-18.47	-18.37
EISJ033218.45-274757.2	1	1	1040109	0.549	23.45	-17.55	-18.27	-18.73	-19.38	-19.32
EISJ033220.40-274735.3	2	1	1040110	0.769	24.72	56.65	-18.01	-18.94	-17.44	-17.26
EISJ033236.76-274843.7	1	1	1040111	0.215	23.89	-16.43	-16.27	-16.09	-15.91	-15.77
EISJ033235.77-274759.0	1	2	1040112	0.665	20.46	-19.46	-21.64	-22.57	-23.40	-23.35
EISJ033224.87-274706.5	1	1	1040113	0.363	20.48	-18.48	-19.69	-20.53	-21.32	-21.25
EISJ033228.00-274639.3	1	1	1040115	0.249	19.40	-17.63	-19.59	-20.52	-22.07	-22.04
EISJ033246.95-274903.9	3	1	1040121	0.777	24.65	-17.69	-18.15	-18.13	-18.77	-18.44
EISJ033242.33-274950.6	1	1	1040122	0.458	20.47	-18.83	-20.32	-21.25	-22.01	-21.93
EISJ033239.56-274928.6	1	2	1040123	0.664	21.21	-19.07	-20.88	-21.82	-22.62	-22.54
EISJ033247.05-275053.4	2	1	1040125	0.365	22.07	-17.25	-18.28	-18.98	-19.51	-19.41
EISJ033237.40-275014.0	2	1	1040126	0.258	23.36	-16.59	-16.92	-16.96	-17.74	-17.51
EISJ033245.58-274936.4	1	2	1040129	0.678	21.66	-19.19	-20.53	-21.41	-22.33	-22.29
EISJ033231.78-274851.3	1	1	2010001	0.948	23.14	55.29	-20.85	-21.78	-21.94	-21.85
EISJ033227.62-274938.7	2	1	2010002	0.231	20.19	-18.19	-19.12	-19.67	-19.94	-19.81
EISJ033248.89-274753.1	2	1	2010004	0.566	24.15	-17.62	-17.96	-17.93	-18.84	-18.77
GASJ033222.64-275015.2	1	2	2010005	0.529	22.03	-18.06	-19.32	-20.14	-20.89	-20.80
EISJ033233.23-274920.9	2	1	2010006	0.204	22.13	-14.87	-16.32	-17.25	-18.00	-17.74
EISJ033226.62-275002.0	1	1	2010008	0.730	22.20	-19.66	-20.39	-20.80	-21.74	-21.66
EISJ033231.73-274954.4	2	1	2010011	0.774	23.60	-17.90	-19.17	-19.84	-20.97	-20.90
EISJ033249.41-274828.4	2	1	2010012	0.507	18.45	-21.54	-22.71	-23.60	-23.95	-23.91
EISJ033225.26-275033.5	2	1	2010013	0.174	22.40	-15.98	-16.59	-16.88	-17.46	-17.30
EISJ033235.63-274944.1	1	1	2010014	0.542	21.18	-19.50	-20.40	-21.01	-21.47	-21.38
EISJ033232.70-275011.5	1	2	2010016	0.662	20.59	-19.68	-21.49	-22.43	-23.25	-23.23
EISJ033247.99-274855.9	1	1	2010017	0.233	20.51	-17.33	-18.51	-19.29	-19.96	-19.87
EISJ033244.05-275009.8	1	1	2010018	0.698	22.64	-19.27	-19.88	-20.03	-20.61	-20.50
EISJ033236.61-275003.8	2	2	2010020	0.719	22.60	-19.25	-19.97	-20.26	-20.99	-20.89
EISJ033248.92-274905.4	1	1	2010021	0.164	21.46	-14.99	-16.43	-17.37	-18.13	-17.99
EISJ033219.05-275144.0	1	1	2010023	0.276	21.34	-16.92	-18.07	-18.90	-19.45	-19.35
EISJ033220.50-275143.9	1	1	2010026	0.674	22.38	-19.00	-19.93	-20.43	-20.72	-20.63
EISJ033224.16-275134.1	1	1	2010027	0.583	23.60	-17.53	-18.34	-18.72	-19.26	-19.10
EISJ033233.09-275111.4	2	2	2010031	0.625	22.63	-19.04	-19.60	-19.80	-20.26	-20.08
EISJ033245.51-275018.4	1	1	2010034	1.572	23.73	-21.66	-22.65	-23.26	-22.08	-21.98
EISJ033244.87-275028.4	1	1	2010036	0.779	22.00	-20.30	-20.80	-20.89	-21.44	-21.30
EISJ033229.19-275153.3	1	1	2010037	0.506	23.61	-17.48	-18.05	-18.30	-19.02	-18.93
EISJ033245.52-275031.2	2	1	2010038	0.559	23.12	-17.87	-18.64	-19.12	-19.52	-19.41
EISJ033220.87-275255.3	2	1	2010039	0.826	23.15	-19.17	-19.86	-20.20	-20.65	-20.51
EISJ033242.10-275109.6	2	1	2010041	0.958	23.45	-19.60	-20.08	-20.20	-20.34	-20.01
EISJ033244.44-275119.7	1	1	2010042	0.380	23.71	-15.52	-16.68	-17.44	-17.84	-17.43
EISJ033252.33-275052.1	2	2	2010043	0.510	21.80	-17.45	-19.35	-20.28	-21.67	-21.64
EISJ033240.41-275155.9	1	1	2010045	0.674	23.08	-18.79	-19.33	-19.53	-20.22	-20.13
EISJ033230.61-275254.0	2	1	2010047	1.013	23.53	-19.50	-20.47	-21.00	-21.81	-21.72
EISJ033243.01-275152.9	2	2	2010048	0.503	22.91	-18.13	-18.70	-18.99	-18.90	-18.79
EISJ033230.18-275306.1	1	1	2010050	0.640	21.09	-20.64	-21.18	-21.42	-21.61	-21.51
EISJ033252.88-275114.9	3	1	2010052	1.121	21.33	-22.15	-23.51	-24.30	-24.04	-23.96
EISJ033244.55-275225.3	2	1	2010056	0.173	22.52	-14.16	-15.51	-16.44	-17.40	-17.32
EISJ033233.38-275333.6	1	1	2010058	0.679	23.27	-18.97	-19.25	-19.17	-18.96	-18.63
EISJ033250.73-275225.5	1	1	2010061	0.293	20.63	-17.84	-18.99	-19.78	-20.40	-20.31
EISJ033240.82-275343.7	1	1	2010065	0.972	22.11	-20.88	-21.69	-22.22	-22.21	-22.11
EISJ033240.21-275416.5	1	1	2010067	0.679	22.92	-18.86	-19.51	-19.71	-20.00	-19.80
EISJ033251.18-275308.7	3	1	2010070	0.977	22.16	-20.82	-21.66	-22.20	-22.46	-22.37

Table 2. Cont...

ID	T ^a	Q ^a	IntID ^b	z	I _{iso} ^c	M _U	M _B	M _V	M _J	M _K
EISJ033248.70-274946.5	3	1	2010087	1.368	23.55	-21.03	-21.92	-22.42	-22.47	-22.38
EISJ033251.60-275017.9	1	1	2010088	0.848	21.26	-21.26	-21.80	-21.92	-22.42	-22.27
EISJ033249.68-275053.4	2	1	2010089	0.899	23.32	-19.47	-19.95	-20.04	-20.17	-19.83
EISJ033222.48-274934.8	2	2	2010091	0.553	21.94	-17.30	-19.48	-20.41	-22.36	-22.34
EISJ033224.74-274931.8	3	1	2010092	1.582	23.79	-21.51	-22.21	-22.67	-22.45	-22.36
EISJ033223.44-275024.9	2	1	2010093	1.535	23.11	-21.89	-22.45	-22.74	-21.59	-21.23
EISJ033222.61-275232.0	1	1	2010096	0.755	21.49	-20.38	-21.20	-21.61	-22.17	-22.07
EISJ033239.13-275501.0	2	1	2010101	1.120	24.42	-19.57	-18.96	-18.55	-20.01	-19.78
EISJ033222.93-275434.5	2	1	2010110	1.237	20.77	-22.44	-24.86	-25.79	-24.85	-24.76
EISJ033226.88-275423.4	2	1	2010111	0.613	21.17	-18.77	-20.63	-21.56	-22.22	-22.14
EISJ033223.27-275101.9	1	1	2010119	1.069	22.27	-19.63	-22.48	-23.41	-23.15	-23.06
EISJ033233.32-275317.2	2	1	2010120	0.149	20.68	-16.32	-17.34	-18.04	-18.38	-18.22
EISJ033229.66-275343.1	2	1	2010121	0.268	21.74	-15.24	-17.44	-18.38	-18.97	-18.55
EISJ033223.84-275407.4	2	1	2010122	1.079	20.94	54.43	-23.88	-24.81	-19.29	-19.06
EISJ033239.73-275154.9	1	1	2010124	0.413	20.76	-19.20	-20.10	-20.64	-21.04	-20.94
EISJ033248.15-274845.2	2	2	2010133	0.672	21.65	-18.45	-20.49	-21.42	-22.32	-22.28
EISJ033239.48-275031.9	1	2	2010137	0.586	21.41	-18.08	-20.22	-21.15	-22.20	-22.15
EISJ033221.88-275243.2	3	1	2010139	1.300	24.52	-19.81	-20.67	-21.13	-20.46	-20.30
EISJ033221.45-275151.9	1	1	2010140	0.827	22.03	-20.43	-20.95	-21.04	-21.48	-21.29
EISJ033208.45-274146.1	1	2	2020001	0.736	21.52	-19.01	-20.99	-21.93	-22.61	-22.56
EISJ033204.90-274216.6	2	1	2020005	0.746	22.28	-18.83	-20.30	-21.21	-21.90	-21.84
EISJ033214.59-274128.6	2	1	2020006	0.354	22.41	-15.38	-17.59	-18.52	-18.98	-18.55
EISJ033231.19-274017.8	2	2	2020010	0.645	20.72	-20.15	-21.31	-22.15	99.99	99.99
EISJ033220.77-274115.1	2	2	2020012	0.476	23.09	-17.00	-18.02	-18.73	-19.06	-18.66
EISJ033233.03-274017.0	3	1	2020013	1.077	23.56	-19.93	-20.52	-20.72	99.99	99.99
EISJ033224.99-274101.7	2	1	2020015	0.569	21.14	-18.80	-20.38	-21.31	-20.02	-20.00
EISJ033225.87-274104.3	1	1	2020017	0.690	23.70	-18.27	-18.79	-18.94	-18.44	-18.42
EISJ033208.44-274247.3	2	1	2020018	0.181	22.90	-16.31	-16.65	-16.63	-16.36	-15.89
EISJ033222.58-274141.2	2	1	2020019	0.596	20.96	-18.85	-20.73	-21.66	-22.11	-22.02
EISJ033233.24-274050.6	1	1	2020020	0.738	23.48	-18.69	-19.19	-19.30	99.99	99.99
EISJ033209.71-274248.5	1	2	2020021	0.689	20.22	-19.56	-22.02	-22.96	-23.58	-23.55
EISJ033213.25-274241.0	3	1	2020023	0.071	19.58	-13.93	-16.25	-17.18	-18.91	-18.89
EISJ033226.60-274135.9	1	2	2020024	0.538	23.32	-16.85	-18.04	-18.92	-20.36	-20.30
EISJ03236.52-274049.9	3	1	2020025	0.939	21.76	-21.07	-21.83	-22.29	99.99	99.99
EISJ033208.38-274310.3	1	1	2020026	0.740	23.24	-19.35	-19.46	-19.37	-20.48	-20.37
EISJ033235.86-274059.8	1	1	2020028	0.608	21.41	-18.32	-20.36	-21.29	99.99	99.99
EISJ033207.39-274322.0	2	1	2020029	0.669	23.80	-18.89	-18.71	-18.58	-19.33	-19.24
EISJ033218.54-274230.3	2	1	2020030	0.349	22.15	-17.08	-18.10	-18.77	-17.58	-17.19
EISJ033226.82-274156.6	1	1	2020033	0.740	22.95	-19.88	-19.78	-19.45	-20.27	-19.88
EISJ033215.39-274259.3	2	1	2020035	0.259	24.59	-16.75	-16.27	-15.93	-16.18	-15.66
EISJ033226.33-274209.9	1	1	2020036	0.938	22.84	-20.25	-20.57	-20.61	-20.44	-20.00
EISJ033236.26-274122.2	2	1	2020037	0.591	22.71	-17.80	-19.04	-19.81	-20.69	-20.60
EISJ033208.01-274346.3	2	1	2020038	0.605	21.90	-19.04	-19.98	-20.66	-21.66	-21.63
EISJ033217.63-274257.6	1	1	2020039	0.650	22.46	-18.99	-19.78	-20.19	-21.23	-21.15
EISJ033237.36-274126.3	1	2	2020040	0.673	19.05	-21.18	-23.10	-24.03	-24.30	-24.24
EISJ033207.17-274356.2	3	1	2020041	1.373	22.60	-22.05	-23.08	-23.69	-23.65	-23.57
EISJ033217.37-274307.5	1	1	2020042	0.649	21.10	-20.39	-21.15	-21.53	-21.76	-21.65
EISJ033233.13-274155.3	3	1	2020043	0.954	23.40	-19.60	-20.10	-20.19	-20.95	-20.78
EISJ033218.64-274317.5	1	1	2020047	0.736	23.38	-18.60	-19.27	-19.43	-19.85	-19.62
EISJ033229.57-274224.6	2	1	2020048	0.977	23.61	-19.55	-19.86	-19.81	-20.26	-20.11
EISJ033210.92-274415.1	1	3	2020049	1.621	22.32	-23.11	-23.93	-24.44	-23.81	-23.71
EISJ033233.91-274238.1	1	1	2020055	0.624	21.10	-20.15	-20.99	-21.47	-21.91	-21.82
EISJ033225.90-274334.1	2	1	2020057	0.263	22.82	-15.65	-16.66	-17.34	-18.25	-18.17
EISJ033227.59-274331.6	1	2	2020059	0.607	22.73	-18.52	-19.27	-19.75	-20.07	-19.98
GASJ033211.03-274456.0	3	1	2020060	0.832	20.11	-21.26	-22.91	-23.16	-22.37	-22.28
EISJ033223.39-274357.0	2	1	2020061	0.297	23.74	-16.07	-16.54	-16.83	-17.30	-17.22
EISJ033236.22-274258.3	3	1	2020062	0.973	21.00	-22.06	-22.58	-22.70	-22.54	-22.33
EISJ033211.70-274507.7	2	1	2020064	0.679	22.47	-19.18	-19.93	-20.22	-19.88	-19.78
EISJ033219.26-274439.1	1	1	2020067	0.220	22.18	-16.59	-17.24	-17.62	-17.77	-17.63
EISJ033230.04-274347.4	2	2	2020068	0.675	19.85	-21.43	-22.35	-23.17	-23.59	-23.52
EISJ033209.78-274529.5	2	1	2020069	0.537	22.55	-17.99	-18.95	-19.63	-20.09	-20.01
GASJ033221.32-274436.4	1	2	2020070	0.526	19.50	-19.50	-21.75	-22.68	-23.68	-23.66
EISJ033239.68-274306.8	1	1	2020071	0.947	23.56	-19.87	-19.63	-19.30	-20.21	-20.01
EISJ033213.83-274525.8	2	1	2020074	0.964	23.36	-18.73	-20.72	-21.62	-23.06	-23.04
EISJ033213.14-274535.2	1	1	2020075	1.102	23.03	-20.59	-21.12	-21.27	-21.19	-21.04
EISJ033227.31-274428.8	2	1	2020076	0.209	19.95	-17.58	-18.77	-19.56	-20.18	-20.10
EISJ033240.37-274325.0	2	1	2020077	1.249	22.76	-21.48	-22.09	-22.38	-21.03	-20.84
EISJ033221.44-274502.6	2	1	2020078	0.947	23.88	-18.20	-19.84	-20.45	-20.64	-20.55
EISJ033236.57-274349.8	2	2	2020079	0.456	22.80	-16.33	-17.97	-18.91	-19.10	-18.64
EISJ033232.76-274415.8	3	1	2020082	1.230	23.35	-20.70	-21.50	-21.89	-21.47	-21.34
EISJ033214.98-274554.2	3	1	2020083	1.226	22.98	-20.99	-21.48	-21.50	-20.54	-20.22
EISJ033236.34-274407.7	2	1	2020084	0.273	23.18	-16.36	-16.83	-17.17	-17.51	-17.41
EISJ033216.85-274551.3	1	1	2020085	1.022	23.42	-19.90	-20.10	-19.98	-20.06	-19.87
EISJ033235.46-274421.4	2	2	2020086	0.894	22.67	-19.32	-20.92	-21.80	-21.83	-21.74
EISJ033211.58-274623.1	1	1	2020087	1.011	22.34	-20.89	-21.45	-21.65	-21.80	-21.69
EISJ033218.46-274556.1	2	2	2020089	0.737	20.97	-19.40	-21.55	-22.48	-23.30	-23.27
EISJ033220.32-274555.0	2	1	2020092	0.232	20.31	-17.89	-18.78	-19.51	-19.98	-19.89
EISJ033214.04-274634.4	1	1	2020094	0.832	23.31	-17.99	-19.81	-20.55	-21.62	-21.58
EISJ033227.41-274549.7	1	1	2020097	0.727	23.36	-18.59	-19.26	-19.42	-20.42	-20.14
EISJ033225.12-274606.2	1	1	2020098	0.733	22.01	-20.06	-20.65	-20.73	-20.64	-20.53
EISJ033213.48-274710.6	2	1	2020099	0.083	23.72	-13.77	-14.04	-14.04	-14.76	-14.74
EISJ033229.57-274600.3	1	1	2020101	0.335	22.52	-17.31	-17.95	-18.33	-18.84	-18.70
EISJ033241.00-274504.5	1	1	2020102	0.832	23.43	-18.96	-19.57	-19.65	-21.20	-21.11
EISJ033221.70-274650.7	1	1	2020104	1.018	23.16	-20.00	-20.69	-20.93	-20.56	-20.21

Table 2. Cont...

ID	T ^a	Q ^a	IntID ^b	z	I _{isp} ^c	M _U	M _B	M _V	M _J	M _K
EISJ033218.87-274734.5	2	2	2020111	0.733	22.29	-18.07	-20.21	-21.14	-22.04	-22.01
EISJ033233.55-274623.5	3	1	2020112	0.337	21.25	-17.28	-18.61	-19.53	-20.37	-20.28
EISJ033220.49-274732.5	2	1	2020113	0.599	21.97	-17.88	-19.74	-20.67	-22.20	-22.18
EISJ033209.43-274135.2	1	2	2020117	0.736	21.95	-18.40	-20.56	-21.50	-22.03	-21.96
EISJ033219.39-274051.8	1	1	2020118	0.761	20.82	-20.46	-21.85	-22.77	99.99	99.99
EISJ033238.27-274455.4	2	1	2020126	0.656	21.48	-18.62	-20.57	-21.50	-22.27	-22.19
EISJ033238.60-274500.2	2	1	2020127	0.981	23.83	-19.28	-19.80	-19.96	-20.94	-20.84
EISJ033240.92-274541.2	2	1	2020129	0.151	21.58	-16.01	-16.80	-17.27	-17.74	-17.52
EISJ033225.99-274507.5	2	1	2020131	0.349	22.26	-17.84	-18.37	-18.70	-18.35	-18.26
EISJ033229.99-274530.0	1	3	2020132	1.220	21.11	-22.86	-23.51	-23.66	-23.77	-23.68
EISJ033212.08-274424.7	1	1	2020133	0.842	24.08	-18.67	-18.94	-18.96	-19.58	-19.47
EISJ033227.86-274450.1	2	1	2020135	0.740	24.92	-17.13	-17.78	-17.69	-18.28	-17.89
EISJ033243.97-274503.9	1	1	2020137	0.536	22.49	-18.20	-19.11	-19.64	-20.17	-20.08
EISJ033134.06-274353.5	2	2	2030001	0.525	21.53	-18.02	-19.71	-20.65	99.99	99.99
EISJ033127.83-274429.9	1	1	2030003	0.216	20.66	-17.76	-18.45	-19.02	99.99	99.99
EISJ033142.60-274318.2	1	1	2030004	0.181	20.35	-16.64	-17.89	-18.77	99.99	99.99
EISJ033133.32-274408.6	2	2	2030006	0.332	20.62	-18.79	-19.65	-20.18	99.99	99.99
EISJ033145.69-274308.1	1	2	2030007	0.444	21.57	-18.27	-19.33	-20.04	99.99	99.99
EISJ033120.17-274521.9	2	2	2030008	0.541	22.27	-17.99	-19.19	-19.95	99.99	99.99
EISJ033135.15-274409.6	2	1	2030009	0.563	21.91	-18.39	-19.61	-20.48	99.99	99.99
EISJ033128.69-274514.6	2	2	2030015	0.804	20.74	-20.53	-22.22	-23.16	99.99	99.99
EISJ033135.14-274448.5	1	1	2030017	0.194	22.45	-15.10	-16.14	-16.90	99.99	99.99
EISJ033124.05-274551.8	3	1	2030019	1.218	22.68	-21.36	-22.27	-22.82	99.99	99.99
EISJ033151.44-274337.3	1	1	2030021	1.049	22.80	-20.57	-21.13	-21.28	99.99	99.99
EISJ033141.13-274442.8	1	1	2030024	0.804	21.99	-20.13	-20.93	-21.33	99.99	99.99
EISJ033150.56-274355.1	1	1	2030025	0.684	22.93	-18.42	-19.39	-20.00	99.99	99.99
EISJ033122.08-274622.5	1	2	2030026	0.502	20.49	-18.59	-20.61	-21.54	99.99	99.99
EISJ033150.86-274401.8	3	1	2030028	0.629	23.14	-18.48	-19.06	-19.35	99.99	99.99
EISJ033124.10-274627.6	2	2	2030031	0.679	22.40	-17.86	-19.78	-20.72	99.99	99.99
EISJ033133.69-274559.1	2	1	2030035	0.525	21.90	-18.31	-19.45	-20.23	99.99	99.99
EISJ033123.40-274656.6	3	1	2030036	0.394	21.87	-18.06	-18.92	-19.40	99.99	99.99
EISJ033144.59-274515.7	3	1	2030038	0.730	20.69	-20.04	-21.79	-22.72	99.99	99.99
EISJ033134.95-274607.2	1	1	2030040	0.606	21.64	-19.62	-20.38	-20.81	99.99	99.99
EISJ033144.66-274519.5	1	1	2030041	0.220	18.72	-18.27	-19.93	-20.86	99.99	99.99
EISJ033144.06-274529.2	1	1	2030043	0.180	20.49	-16.67	-17.90	-18.67	99.99	99.99
EISJ033140.10-274553.6	1	1	2030044	0.603	20.86	-19.93	-20.99	-21.70	99.99	99.99
EISJ033153.48-274458.5	1	1	2030047	0.555	23.01	-18.63	-19.04	-19.04	99.99	99.99
EISJ033142.50-274559.3	1	1	2030049	0.059	19.98	-15.14	-16.04	-16.62	99.99	99.99
EISJ033126.64-274722.7	1	1	2030051	0.801	22.97	-19.00	-19.95	-20.52	99.99	99.99
EISJ033149.74-274531.8	1	1	2030053	0.146	20.91	-16.42	-17.33	-17.84	99.99	99.99
EISJ033127.19-274726.0	2	1	2030054	0.679	22.80	-19.19	-19.68	-19.74	99.99	99.99
EISJ033140.71-274621.5	1	1	2030055	0.672	22.09	-18.79	-20.08	-20.94	99.99	99.99
EISJ033152.55-274524.9	1	2	2030056	0.732	22.37	-18.35	-20.12	-21.06	99.99	99.99
EISJ033138.85-274637.5	1	2	2030057	0.674	21.42	-19.29	-20.73	-21.67	99.99	99.99
EISJ033135.64-274701.8	1	1	2030059	0.717	22.31	-19.64	-20.27	-20.47	99.99	99.99
EISJ033154.71-274537.9	3	1	2030062	1.033	24.12	-19.29	-19.52	-19.45	99.99	99.99
EISJ033131.55-274737.3	1	1	2030063	0.223	19.40	-17.98	-19.29	-20.22	99.99	99.99
EISJ033138.15-274712.0	3	1	2030066	1.040	20.80	-22.43	-23.18	-23.47	99.99	99.99
EISJ033151.77-274606.3	2	2	2030067	0.743	21.37	-20.25	-21.21	-22.00	99.99	99.99
EISJ033127.40-274814.5	1	2	2030068	0.677	22.75	-18.08	-19.43	-20.34	99.99	99.99
EISJ033125.63-274829.3	1	1	2030071	0.562	22.01	-18.76	-19.67	-20.29	99.99	99.99
EISJ033153.25-274619.4	2	2	2030073	0.733	20.47	-20.35	-22.03	-22.96	99.99	99.99
EISJ033154.76-274619.1	2	1	2030075	0.602	22.84	-17.44	-18.89	-19.81	99.99	99.99
EISJ033133.76-274822.3	1	1	2030077	0.672	22.54	-19.34	-19.89	-20.01	99.99	99.99
EISJ033152.62-274652.0	1	2	2030078	0.766	22.43	-19.18	-20.29	-20.94	99.99	99.99
EISJ033144.43-274802.4	1	1	2030083	0.180	19.53	-16.91	-18.60	-19.54	99.99	99.99
EISJ033137.25-274844.5	1	1	2030084	0.955	22.05	-20.77	-21.71	-22.33	99.99	99.99
EISJ033128.61-274934.7	1	2	2030086	0.515	21.23	-17.50	-19.95	-20.88	99.99	99.99
EISJ033145.74-274818.5	1	2	2030090	0.616	20.23	-19.53	-21.59	-22.52	99.99	99.99
EISJ033155.43-274731.6	1	1	2030091	0.677	22.33	-19.30	-20.03	-20.44	99.99	99.99
EISJ033137.68-274905.1	1	2	2030092	0.682	22.30	-17.91	-19.90	-20.83	99.99	99.99
EISJ033128.21-274958.9	1	1	2030094	0.287	21.45	-16.52	-17.93	-18.86	99.99	99.99
EISJ033137.77-274914.5	2	2	2030095	0.904	23.05	-19.66	-20.23	-20.29	99.99	99.99
EISJ033159.11-274744.7	1	2	2030100	0.549	21.06	-18.44	-20.34	-21.27	99.99	99.99
EISJ033146.53-274851.0	3	1	2030102	0.896	23.16	-19.83	-20.06	-20.06	99.99	99.99
EISJ033129.42-275021.4	3	1	2030103	0.900	23.03	-19.59	-20.28	-20.48	99.99	99.99
EISJ033145.25-274904.9	3	1	2030104	0.839	22.46	-19.96	-20.57	-20.69	99.99	99.99
EISJ033138.51-274944.3	2	2	2030106	0.676	21.29	-19.02	-20.87	-21.81	99.99	99.99
EISJ033151.10-274844.1	3	1	2030107	1.109	22.64	-20.85	-21.69	-22.04	99.99	99.99
EISJ033138.65-274950.3	1	1	2030108	0.300	20.90	-17.96	-18.96	-19.61	99.99	99.99
EISJ033131.61-275037.9	1	1	2030109	0.335	19.94	-19.23	-20.22	-20.87	99.99	99.99
EISJ033150.97-274906.1	2	2	2030110	0.591	21.61	-19.06	-20.15	-20.91	99.99	99.99
EISJ033131.15-275049.3	2	2	2030111	0.678	20.33	-20.73	-21.86	-22.74	99.99	99.99
EISJ033200.94-274842.1	1	1	2030118	0.534	23.15	-18.29	-18.73	-18.85	99.99	99.99
EISJ033132.29-275109.3	2	1	2030119	0.572	22.86	-18.27	-18.99	-19.43	99.99	99.99
EISJ033147.86-274954.6	3	1	2030120	1.000	23.03	-20.27	-20.61	-20.65	99.99	99.99
EISJ033158.21-274905.1	2	2	2030121	0.536	20.93	-19.80	-20.51	-21.26	99.99	99.99
EISJ033139.39-275042.4	1	1	2030122	0.678	23.32	-18.18	-19.02	-19.49	99.99	99.99
EISJ033133.33-274818.4	3	1	2030124	0.819	20.91	-21.03	-22.12	-22.82	99.99	99.99
EISJ033148.44-274549.3	1	2	2030139	0.735	22.62	-18.00	-19.89	-20.80	99.99	99.99
EISJ033153.37-274412.5	1	1	2030141	0.684	22.61	-19.36	-19.84	-20.04	99.99	99.99
EISJ033151.19-274852.3	2	1	2030148	0.997	22.31	-20.85	-21.44	-21.69	99.99	99.99
EISJ033147.90-274813.2	1	1	2030152	0.652	22.72	-18.72	-19.50	-19.98	99.99	99.99
EISJ033157.12-274744.7	2	1	2030153	0.746	23.65	-17.90	-18.98	-19.56	99.99	99.99

Table 2. Cont...

ID	T ^a	Q ^a	IntID ^b	z	I _{ISD} ^c	M _U	M _B	M _V	M _J	M _K
EISJ033153.91-275223.8	2	2	2040009	0.821	21.69	-19.26	-21.39	-22.33	99.99	99.99
EISJ033200.44-275228.8	2	2	2040016	0.632	21.13	-18.72	-20.79	-21.72	99.99	99.99
EISJ033138.55-275420.7	3	1	2040017	0.747	22.27	-19.84	-20.42	-20.57	99.99	99.99
EISJ033149.09-275328.2	2	1	2040018	0.617	22.02	-18.59	-19.86	-20.67	99.99	99.99
EISJ033137.27-275450.6	1	1	2040022	0.703	22.81	-19.19	-19.75	-19.81	99.99	99.99
EISJ033155.14-275338.1	2	2	2040027	0.216	21.00	-17.77	-18.50	-18.79	99.99	99.99
EISJ033143.32-275441.7	1	1	2040028	0.215	22.26	-16.77	-17.30	-17.54	99.99	99.99
EISJ033156.86-275338.5	1	2	2040029	0.657	22.12	-18.37	-19.94	-20.87	99.99	99.99
EISJ033138.58-275528.2	1	1	2040035	0.300	22.82	-16.31	-17.18	-17.71	99.99	99.99
EISJ033150.45-275428.3	2	2	2040036	0.560	20.79	-18.64	-20.67	-21.61	99.99	99.99
EISJ033155.90-275420.8	2	1	2040041	1.100	22.40	-21.19	-21.96	-22.42	99.99	99.99
EISJ033207.21-275325.6	2	1	2040042	0.314	22.61	-16.16	-17.27	-18.01	99.99	99.99
EISJ033145.51-275535.2	2	1	2040044	0.863	22.39	-20.19	-20.77	-21.01	99.99	99.99
EISJ033156.03-275453.8	1	2	2040048	0.734	20.79	-20.37	-21.72	-22.63	99.99	99.99
EISJ033206.99-275359.2	1	2	2040049	0.687	21.36	-19.00	-20.87	-21.80	99.99	99.99
EISJ033138.06-275627.6	1	1	2040050	0.678	21.56	-20.03	-20.78	-21.25	99.99	99.99
EISJ033157.52-275454.6	2	1	2040051	0.629	21.94	-17.69	-19.96	-20.89	99.99	99.99
EISJ033143.77-275614.2	1	1	2040054	1.317	21.85	-22.57	-23.27	-23.60	99.99	99.99
EISJ033140.95-275644.0	1	1	2040060	0.123	20.60	-15.35	-16.64	-17.53	99.99	99.99
EISJ033138.31-275704.6	1	1	2040062	0.486	21.89	-18.55	-19.40	-19.97	99.99	99.99
EISJ033204.61-275700.2	1	2	2040064	0.522	20.45	-18.71	-20.77	-21.71	99.99	99.99
EISJ033144.97-275641.0	1	2	2040065	0.719	21.00	-19.22	-21.41	-22.35	99.99	99.99
EISJ033159.93-275528.0	1	2	2040066	0.691	21.19	-19.03	-21.06	-22.00	99.99	99.99
EISJ033148.71-275628.6	1	1	2040067	0.290	22.70	-14.80	-16.70	-17.64	99.99	99.99
EISJ033208.44-275455.1	1	2	2040068	0.689	20.94	-19.39	-21.30	-22.24	99.99	99.99
EISJ033143.19-275704.9	1	1	2040069	0.258	21.04	-17.42	-18.39	-19.07	99.99	99.99
EISJ033148.34-275650.1	3	1	2040071	1.220	21.71	-22.37	-23.20	-23.70	99.99	99.99
EISJ033157.84-275605.2	2	1	2040072	0.737	21.60	-19.65	-20.94	-21.79	99.99	99.99
EISJ033210.65-275502.5	2	2	2040073	0.525	21.08	-18.00	-20.16	-21.10	99.99	99.99
EISJ033209.57-275516.4	2	2	2040076	0.703	22.94	-17.75	-19.38	-20.31	99.99	99.99
EISJ033152.41-275655.2	1	1	2040080	0.745	22.26	-19.86	-20.43	-20.55	99.99	99.99
EISJ033154.99-275651.5	1	1	2040082	0.745	21.93	-19.81	-20.70	-21.25	99.99	99.99
EISJ033154.49-275659.9	1	1	2040085	0.321	21.32	-17.69	-18.69	-19.37	99.99	99.99
EISJ033207.48-275557.3	1	1	2040086	0.698	22.40	-18.81	-19.96	-20.66	99.99	99.99
EISJ033203.64-275622.8	1	1	2040088	0.318	22.39	-16.65	-17.63	-18.28	99.99	99.99
EISJ033204.18-275626.5	1	1	2040089	0.625	22.20	-19.33	-19.96	-20.30	99.99	99.99
EISJ033206.39-275622.0	2	2	2040091	0.415	19.64	-18.68	-20.84	-21.78	99.99	99.99
EISJ033151.07-275747.7	2	2	2040093	0.749	21.12	-19.69	-21.47	-22.41	99.99	99.99
EISJ033203.29-275648.3	1	1	2040094	0.680	22.20	-19.79	-20.28	-20.34	99.99	99.99
EISJ033149.03-275808.8	2	1	2040098	0.281	22.32	-16.28	-17.31	-18.01	99.99	99.99
EISJ033210.99-275623.8	1	1	2040099	0.374	21.88	-18.55	-19.12	-19.27	99.99	99.99
EISJ033203.91-275704.4	1	1	2040101	0.300	19.28	-18.83	-20.22	-21.15	99.99	99.99
EISJ033159.85-275731.2	1	1	2040103	0.680	21.25	-20.18	-21.06	-21.64	99.99	99.99
EISJ033210.87-275638.3	2	2	2040104	0.553	19.85	-20.20	-21.59	-22.49	99.99	99.99
EISJ033158.01-275825.5	2	2	2040105	0.529	23.04	-18.01	-18.70	-18.99	99.99	99.99
EISJ033200.29-275800.9	2	2	2040107	0.653	20.68	-19.61	-21.35	-22.29	99.99	99.99
EISJ033212.98-275714.5	1	1	2040111	0.367	20.94	-18.41	-19.45	-20.12	99.99	99.99
EISJ033146.68-275927.5	1	1	2040112	0.214	20.02	-17.52	-18.73	-19.55	99.99	99.99
EISJ033156.94-275836.4	1	1	2040113	0.785	22.88	-19.04	-19.95	-20.56	99.99	99.99
EISJ033148.72-275858.4	2	1	2040116	0.683	20.12	-20.11	-22.09	-23.02	99.99	99.99
EISJ033203.50-275147.0	1	1	2040122	0.149	19.15	-16.89	-18.50	-19.43	99.99	99.99
EISJ033152.38-275240.0	1	1	2040127	0.658	21.67	-19.63	-20.52	-21.13	99.99	99.99
GASJ033155.00-275150.0	2	1	2040134	0.657	99.99	-20.26	57.93	57.00	99.99	99.99
EISJ033143.02-274756.9	1	4	1010001	0.000	14.45	99.99	99.99	99.99	99.99	99.99
EISJ033133.33-274710.4	1	4	1010002	0.000	20.02	99.99	99.99	99.99	99.99	99.99
EISJ033146.03-274739.8	1	4	1010012	0.000	18.23	99.99	99.99	99.99	99.99	99.99
EISJ033152.51-274659.0	1	4	1010028	0.000	18.89	99.99	99.99	99.99	99.99	99.99
EISJ033143.00-274607.4	1	4	1010031	0.000	20.10	99.99	99.99	99.99	99.99	99.99
EISJ033133.77-274504.3	1	4	1010036	0.000	19.12	99.99	99.99	99.99	99.99	99.99
EISJ033134.48-274502.3	1	4	1010039	0.000	17.76	99.99	99.99	99.99	99.99	99.99
EISJ033205.59-274638.3	1	4	1010051	0.000	20.34	99.99	99.99	99.99	99.99	99.99
EISJ033156.39-274513.1	1	4	1010061	0.000	21.35	99.99	99.99	99.99	99.99	99.99
EISJ033157.43-274424.7	1	4	1010073	0.000	20.28	99.99	99.99	99.99	99.99	99.99
EISJ033140.30-274301.5	1	4	1010074	0.000	16.64	99.99	99.99	99.99	99.99	99.99
EISJ033156.48-274410.9	1	4	1010075	0.000	19.32	99.99	99.99	99.99	99.99	99.99
EISJ033201.71-274417.3	1	4	1010081	0.000	20.17	99.99	99.99	99.99	99.99	99.99
EISJ033140.34-274146.6	1	4	1010097	0.000	19.33	99.99	99.99	99.99	99.99	99.99
EISJ033144.55-274134.2	1	4	1010107	0.000	20.32	99.99	99.99	99.99	99.99	99.99
EISJ033138.80-274460.0	1	4	1010125	0.000	20.36	99.99	99.99	99.99	99.99	99.99
EISJ033134.24-274607.3	1	4	1010130	0.000	22.31	99.99	99.99	99.99	99.99	99.99
EISJ033142.80-274243.3	1	4	1010138	0.000	19.70	99.99	99.99	99.99	99.99	99.99
EISJ033131.87-275531.6	1	4	1020015	0.000	20.21	99.99	99.99	99.99	99.99	99.99
EISJ033126.41-275301.0	1	4	1020044	0.000	18.03	99.99	99.99	99.99	99.99	99.99
EISJ033150.54-275412.0	1	4	1020055	0.000	19.69	99.99	99.99	99.99	99.99	99.99
EISJ033134.56-275247.1	1	4	1020059	0.000	21.32	99.99	99.99	99.99	99.99	99.99
EISJ033124.80-275118.0	1	4	1020069	0.000	20.99	99.99	99.99	99.99	99.99	99.99
EISJ033126.94-275039.7	1	4	1020085	0.000	19.28	99.99	99.99	99.99	99.99	99.99
EISJ033138.68-275000.3	1	4	1020106	0.000	18.54	99.99	99.99	99.99	99.99	99.99
EISJ033132.80-275439.9	2	4	1020109	0.000	21.20	99.99	99.99	99.99	99.99	99.99
EISJ033139.37-275048.2	2	4	1020117	0.000	99.99	99.99	99.99	99.99	99.99	99.99
EISJ033227.08-280038.9	1	4	1030010	0.000	18.02	99.99	99.99	99.99	99.99	99.99
EISJ033221.99-275954.3	2	4	1030017	0.000	20.15	99.99	99.99	99.99	99.99	99.99
EISJ033205.52-275810.9	1	4	1030026	0.000	18.81	99.99	99.99	99.99	99.99	99.99
EISJ033231.98-275847.1	1	4	1030044	0.000	18.22	99.99	99.99	99.99	99.99	99.99

Table 2. Cont...

ID	T ^a	Q ^a	IntID ^b	z	I _{AB} ^c	M _U	M _B	M _V	M _J	M _K
EISJ033233.56-275645.9	1	4	1030084	0.000	21.09	99.99	99.99	99.99	99.99	99.99
EISJ033235.40-275625.7	1	4	1030090	0.000	21.14	99.99	99.99	99.99	99.99	99.99
EISJ033210.17-275406.9	1	4	1030096	0.000	21.40	99.99	99.99	99.99	99.99	99.99
EISJ033221.78-275409.9	1	4	1030112	0.000	19.24	99.99	99.99	99.99	99.99	99.99
EISJ033204.00-275701.8	2	4	1030119	0.000	19.17	99.99	99.99	99.99	99.99	99.99
EISJ033210.51-275547.6	1	4	1030121	0.000	21.62	99.99	99.99	99.99	99.99	99.99
EISJ033217.39-275307.3	1	4	1030126	0.000	22.69	99.99	99.99	99.99	99.99	99.99
EISJ033206.14-275509.6	1	4	1030149	0.000	21.60	99.99	99.99	99.99	99.99	99.99
EISJ033214.36-280017.2	1	4	1030151	0.000	19.15	99.99	99.99	99.99	99.99	99.99
EISJ033230.91-275132.0	1	4	1040003	0.000	20.02	99.99	99.99	99.99	99.99	99.99
EISJ033230.69-275109.2	1	4	1040009	0.000	18.78	99.99	99.99	99.99	99.99	99.99
EISJ033240.88-275122.6	1	4	1040017	0.000	21.74	99.99	99.99	99.99	99.99	99.99
EISJ033232.58-275022.5	1	4	1040023	0.000	19.95	99.99	99.99	99.99	99.99	99.99
EISJ033222.35-274925.7	1	4	1040025	0.000	17.30	99.99	99.99	99.99	99.99	99.99
EISJ033235.07-274844.5	1	4	1040047	0.000	20.86	99.99	99.99	99.99	99.99	99.99
EISJ033253.46-274829.8	1	4	1040066	0.000	18.17	99.99	99.99	99.99	99.99	99.99
EISJ033233.21-274559.1	2	4	1040079	0.000	22.59	99.99	99.99	99.99	99.99	99.99
EISJ033242.77-274608.9	1	4	1040086	0.000	22.61	99.99	99.99	99.99	99.99	99.99
EISJ033241.06-275234.3	1	4	1040092	0.000	20.73	99.99	99.99	99.99	99.99	99.99
EISJ033246.23-275249.3	1	4	1040093	0.000	20.71	99.99	99.99	99.99	99.99	99.99
EISJ033216.90-275031.4	1	4	1040101	0.000	19.81	99.99	99.99	99.99	99.99	99.99
EISJ033246.40-274820.3	1	4	2010007	0.000	21.36	99.99	99.99	99.99	99.99	99.99
EISJ033222.81-275053.4	1	4	2010015	0.000	19.60	99.99	99.99	99.99	99.99	99.99
EISJ033227.14-275049.2	1	4	2010019	0.000	20.12	99.99	99.99	99.99	99.99	99.99
EISJ033233.19-275034.6	1	4	2010024	0.000	20.48	99.99	99.99	99.99	99.99	99.99
EISJ033236.69-275240.4	2	4	2010053	0.000	22.45	99.99	99.99	99.99	99.99	99.99
EISJ03225.58-275504.5	1	4	2010066	0.000	19.38	99.99	99.99	99.99	99.99	99.99
EISJ033249.21-274933.4	2	4	2010084	0.000	22.35	99.99	99.99	99.99	99.99	99.99
EISJ033242.43-274759.1	1	4	2010085	0.000	18.51	99.99	99.99	99.99	99.99	99.99
EISJ033227.18-275556.7	1	4	2010102	0.000	17.54	99.99	99.99	99.99	99.99	99.99
EISJ033236.18-274042.4	1	4	2020022	0.000	18.94	99.99	99.99	99.99	99.99	99.99
EISJ033231.64-274208.1	1	4	2020046	0.000	16.88	99.99	99.99	99.99	99.99	99.99
EISJ033213.95-274406.0	1	4	2020052	0.000	17.81	99.99	99.99	99.99	99.99	99.99
EISJ033210.45-274507.4	1	4	2020063	0.000	15.68	99.99	99.99	99.99	99.99	99.99
EISJ033230.54-274459.6	1	4	2020090	0.000	19.40	99.99	99.99	99.99	99.99	99.99
EISJ033210.49-274641.0	1	4	2020091	0.000	20.21	99.99	99.99	99.99	99.99	99.99
EISJ033220.92-274646.9	1	4	2020103	0.000	21.24	99.99	99.99	99.99	99.99	99.99
EISJ033233.15-274039.2	1	4	2020120	0.000	18.27	99.99	99.99	99.99	99.99	99.99
EISJ03223.79-274123.7	1	4	2020121	0.000	20.71	99.99	99.99	99.99	99.99	99.99
EISJ03226.88-274247.9	1	4	2020123	0.000	22.35	99.99	99.99	99.99	99.99	99.99
EISJ033221.05-274310.2	1	4	2020134	0.000	21.08	99.99	99.99	99.99	99.99	99.99
EISJ033149.27-274302.0	2	4	2030010	0.000	22.41	99.99	99.99	99.99	99.99	99.99
EISJ033136.54-274415.6	2	4	2030012	0.000	22.19	99.99	99.99	99.99	99.99	99.99
EISJ033154.44-274447.9	1	4	2030045	0.000	22.27	99.99	99.99	99.99	99.99	99.99
EISJ033145.60-274615.6	2	4	2030060	0.000	18.51	99.99	99.99	99.99	99.99	99.99
EISJ033141.45-274647.3	1	4	2030064	0.000	18.92	99.99	99.99	99.99	99.99	99.99
EISJ033143.93-274758.9	2	4	2030081	0.000	19.93	99.99	99.99	99.99	99.99	99.99
EISJ033158.09-274709.6	1	4	2030088	0.000	18.72	99.99	99.99	99.99	99.99	99.99
EISJ033154.09-274747.0	1	4	2030093	0.000	19.71	99.99	99.99	99.99	99.99	99.99
EISJ033145.73-274847.5	1	4	2030099	0.000	18.57	99.99	99.99	99.99	99.99	99.99
EISJ033143.29-275000.9	1	4	2030114	0.000	20.18	99.99	99.99	99.99	99.99	99.99
EISJ033157.82-274847.7	2	4	2030115	0.000	20.71	99.99	99.99	99.99	99.99	99.99
EISJ033122.35-274719.6	1	4	2030130	0.000	21.11	99.99	99.99	99.99	99.99	99.99
EISJ033143.27-274719.7	1	4	2030132	0.000	21.23	99.99	99.99	99.99	99.99	99.99
EISJ033156.07-274656.5	1	4	2030137	0.000	18.95	99.99	99.99	99.99	99.99	99.99
EISJ033147.16-275326.1	1	4	2040014	0.000	20.54	99.99	99.99	99.99	99.99	99.99
EISJ033205.79-275157.4	1	4	2040015	0.000	20.20	99.99	99.99	99.99	99.99	99.99
EISJ033146.61-275353.2	1	4	2040020	0.000	18.63	99.99	99.99	99.99	99.99	99.99
EISJ033201.96-275320.2	1	4	2040032	0.000	18.84	99.99	99.99	99.99	99.99	99.99
EISJ033158.88-275504.1	1	4	2040055	0.000	18.95	99.99	99.99	99.99	99.99	99.99
EISJ033156.67-275524.3	1	4	2040058	0.000	20.04	99.99	99.99	99.99	99.99	99.99
EISJ033208.83-275544.8	1	4	2040083	0.000	20.16	99.99	99.99	99.99	99.99	99.99
EISJ033144.73-275909.3	2	4	2040117	0.000	22.22	99.99	99.99	99.99	99.99	99.99
EISJ033202.05-275742.9	2	4	2040118	0.000	20.61	99.99	99.99	99.99	99.99	99.99
EISJ033148.05-275832.0	1	4	2040119	0.000	19.96	99.99	99.99	99.99	99.99	99.99
EISJ033133.68-275358.6	1	4	2040120	0.000	18.58	99.99	99.99	99.99	99.99	99.99
EISJ033206.78-275202.8	1	4	2040123	0.000	20.31	99.99	99.99	99.99	99.99	99.99
EISJ033141.77-275832.7	1	4	2040138	0.000	21.31	99.99	99.99	99.99	99.99	99.99

^a Classification (type=1: emission; type= 2 absorption; type= 3: QSO; type= 4: star) and associated quality of the spectra described in section 2 (Q= 1: insecure; Q= 2: secure; Q= 9: single emission)

^b Internal identifier associated to spectra filename.

^c I_{AB} band photometry from EIS database (Arnouts et al., 2001)

- U, B, V, J and K absolute magnitudes in the AB system estimated following Hammer et al. (2005). 99.99 corresponds to non available quantities.